NANOPETROPHYSICS OF THE NIOBRARA FORMATION

IN BERTHOUD STATE #3 WELL

OF COLORADO, USA

by

RAFAEL ROBERTO VILLEGAS

Presented to the Faculty of the Graduate School of

The University of Texas at Arlington in Partial Fulfillment

of the Requirements

for the Degree of

MASTER OF SCIENCE IN EARTH AND ENVIRONMENTAL SCIENCE

THE UNIVERSITY OF TEXAS AT ARLINGTON

December 2016

Acknowledgements

First and foremost, I would like to thank God for with Him all things are possible. Thank you for having given me the determination and perseverance to peruse my dreams and overcome the hardships that I faced along the way.

I would like to thank my advisor Dr. Q.H. Hu for his guidance and assistance during my time at UTA. The research conducted by Dr. Hu and his research team is on the forefront of understanding unconventional reservoirs. I would also like to thank Dr. Majie Fan and Dr. John Wickham for having served on my committee and their support throughout my time at UTA.

I would like to thank the staff at the USGS core repository in Golden, Colorado for their help and providing samples used throughout this research. Without the donated samples from the USGS this research would not have been possible. There were also several members of the CP3M team which were helpful during my time at UTA: Shawn, Kibria, Tony and Ryan.

I am grateful for the upbringing and motivation provided by my parents Dr. Rafael and Norma Villegas. To my sister Analisa, thank you for your support and insight when I needed it the most. Last, but certainly not least, I would like to thank my wife Karina. Without her support, patience, encouragement and unfaltering love this journey may have never come to fruition.

December 23, 2016

Abstract

NANOPETROPHYSICS OF THE NIOBRARA FORMATION

In BERTHOUD STATE #3 WELL of

COLORADO, USA

Rafael Villegas, MS

The University of Texas at Arlington, 2016

Supervising Professor: Qinhong Hu

The advent of new drilling and completion technologies over the past two decades has made unconventional shale reservoirs the focus of much of the oil and gas exploration and production throughout the United States. Despite large estimated reserves, unconventional reservoirs are typically characterized by low porosity and extremely low matrix permeability, partly accounting for the relatively low recovery rates seen, ranging from 10-15%. Increasing production from unconventional reservoirs requires an understanding of the reservoir's nano-petrophysical properties including pore throat size distribution and edge accessible porosity. Furthermore, an understanding of the relationship between TOC, mineralogy, and pore throat distribution is critical in determining hydrocarbon storage potential and migration pathways, and ultimately recovery rates of the reservoirs.

Similar to many unconventional reservoirs which are prevalent throughout the United States, the Niobrara has been at the forefront of new innovations in hydrocarbon production. Well known as a tight gas reserve, the Niobrara Formation encompasses North Eastern Colorado, Wyoming, Montana, North Western Kansas, and Central Nebraska. The Niobrara was deposited during a major marine transgression of the western interior seaway during the Cretaceous and is characterized by calcareous hemipelagic beds of intervening chalks and marls.

After collecting core samples from 8 units within the Niobrara Formation in Berthoud State #3 Well, this research examined analyses of TOC, XRD, wettability, Mercury Injection Capillary Pressure (MICP), low-pressure nitrogen sorption, and fluid imbibition to determine pore geometry and connectivity within the formation. It was found that illite content plays a key role in pore size distribution and porosity, with a tendency for an increase in 2.8-5 nm pore throats and a decrease in porosity for samples with illite content above 10%. Other finding from wettability studies showed the samples were oil wet source rocks and imbibition studies produced results which suggested low pore connectivity.

Table of Contents

List of Illustrations

List of Tables

Chapter 1

Introduction

Hydrocarbons from shale have been produced since early 1800s, where

nano-darcy permeability was most likely related to natural fractures that allowed

for hydrocarbon transmissibility (Chong et al., 2010). Over time, more research

proved that natural fractures in shales, like those found in the Niobrara, were

actually filled with calcite or quartz, not gas or oil (Chong et al, 2010; Hanley

and VanHorn, 1982). The years (about when?) following early shale oil

discoveries in conventional wells saw steep decline in production of these ultra-

low permeability reservoirs and consequently exploration in "uneconomic"

shales greatly slowed (Anderson et al., 2010).

The relatively recent advent of hydraulic fracturing and horizontal drilling

has caused a resurgence of interest in previously unproductive resource plays. In

order to make unconventional reservoirs a viable option, hydraulic fracturing

attempts to increase the surface area of a formation by inducing or enhancing

natural fractures connected to a well (Anderson et al., 2010). This

unconventional exploration has caused shale plays throughout the country to be

re-evaluated for their economic potential. It has been estimated that there are

over 3.7 trillion barrels of oil in place in various unconventional reservoirs

throughout the country, yet many unconventional reservoirs only produce 10%

of their estimated hydrocarbon potential (Dyni, 2010). This is due in part to factors such as permeability, porosity, and edge accessible pore connectivity. Some of the most productive and most studied shale plays in the United States have been the Bakken, Eagle Ford, and Marcellus (EIA website, monthly report, 2016). The Niobrara Shale in Colorado has recently been an area of focus for many companies looking to mirror the successes seen in other successful shale formations.

<div align="center">Niobrara Formation</div>

Despite similarities between various shale plays, each formation is unique in its own right with varying geologic, geochemical, and geomechanic attributes which all influence the production of hydrocarbons (Anderson et al., 2010). Anderson et al (2010) stated that the ability of a reservoir to be effectively fractured, the capability of a reservoir to sustain commercial production, and the ability of a field to be both economic and environmentally sound are aspects required for a successful completion of an unconventional reservoir.

Although tight oil and gas plays such as the Niobrara are reported to have large amounts of reserves, they have been plagued with production issues. A recent study conducted by Hughes (2014), examining the top seven tight oil plays in the US that account for 89% of current tight oil production, found that only 43% to 64% of their estimated ultimate recovery was achieved in the first

three years. This study also found that steep decline seen in these plays resulted

in a 90% decline in production over that same three-year period. Tight gas plays

had a similar decline rate and saw a decline of 74% to 82% after first three years

of production (Hughes, 2014). Hu et al. (2014) reported that only 10-30% of

estimated gas in place has been recovered from one of the top producing gas

fields in Texas, the Barnett Shale. This decline is most likely attributed to the

ultra-low matrix permeability of shales (Anderson et al., 2010). Despite the

acceptance of steep decline curves seen in tight shale plays, a fundamental

understanding of their mechanisms have rarely been examined (Hu et al., 2014).

This study attempts to investigate the cause of steep decline and low overall

recovery seen in the Niobrara Shale.

Steep decline curves in shale reservoirs have been widely observed, and

the fact that this is the norm rather than the exception may be directly

attributed to poorly connected pore networks. Decline rates of 60% or more are

commonly observed after the first year of production. One of the few solutions

which can successfully combat the steep decline in production is to re-frac

unconventional wells. But re-fracking unconventional wells has several inherent

problems. Re-fracking takes time and is costly, which in turn drives completion

costs higher. Furthermore, the process is merely temporary in terms of

production. Initially upon re-fracking, production rates spike and are once again

favorable; however steep decline quickly returns. This phenomenon seems to be reservoir independent and has been well documented in unconventional plays such as the Barnett, Bakken, Eagle Ford, Marcellus, and Niobrara (Hu, 2015a, Hu, 2015b). In order to determine the root cause of steep decline curves observed in unconventional plays, a better understanding of pore structure, and furthermore pore connectivity, in conjunction with edge accessible porosity is required.

Objectives of Study

The Niobrara Formation in Colorado is an area of special interest to the petroleum industry due to the large amounts of hydrocarbon reserves that are predicted to be held within the formation. The Niobrara Formation has predominantly been an area coveted for its natural gas production and has been well documented as a tight gas reserve (Hanley and VanHorn, 1982). The formation is known for its low permeability and porosity, which has proven difficult for production. Shales, such as the Niobrara, typically exhibit pore sizes in the range of micropore, less than 2 nm, to mesopore, between 2 to 50 nm in size according to to IUPAC classification (Kuila et al., 2013). Other economically important formations such as the Bakken, Eagle Ford, and Barnett shales have been examined for their porosity utilizing various methods, yet to date there

have only been limited studies conducted within the Niobrara to examine these characteristics.

Fully grasping the expanse of the pore structure network and edge accessibility within the Niobrara Shale will give a better understanding as to the fluid flow characteristics of potential hydrocarbons within the formation (Bustin and Bustin, 2012). Mercury injection capillary pressure (MICP) measurements have long been used to determine pore throat size distribution and has the ability to measure pore throat sizes from 3 nm to 300 um in diameter (Kuila et al., 2012).
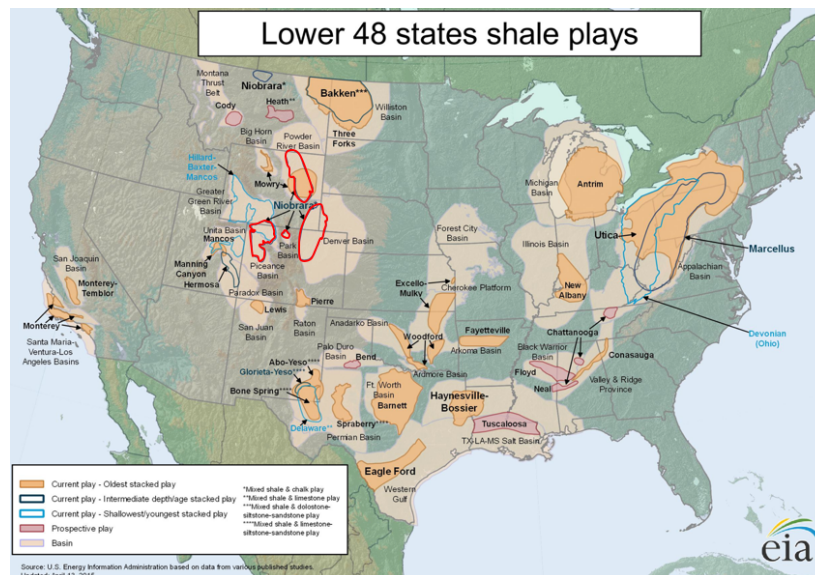
Figure 1 Major US shale plays with the Niobrara highlighted in red (modified from EIA April, 2015)

Chapter 2

Geologic Setting and Petroleum Potential

Geologic Setting

The extent of the Niobrara Shale encompasses North Eastern Colorado,

Wyoming, Montana, North Western Kansas, and Central Nebraska (Fig. 1)

(Brown et al., 1982; EIA, 2015). The major marine transgression of the

Western Interior Seaway (Fig. 2), which extended from the Arctic Ocean to the

Gulf of Mexico, deposited hemipelagic carbonate rich sediments that eventually

formed the Niobrara Shale (Brown et al., 1982).   The western side of the

seaway experienced mountain building during the Late Cretaceous producing an

asymmetric foreland basin (Pratt et al., 1985). As a result of the developing

mountain range, the deeper western portion of the seaway received runoff from

the mountains in the way of coarse siliciclastic sediments (Longman, 1998).

Strong oceanic currents eventually carried away the finer-grained siliciclastic silts

and shales with deposition occurring tens of miles away in the more gently

dipping eastern portion of the seaway (Fig. 3) (Longman, 1998; Kauffman and

Caldwell, 1993; Shurr et al., 1994).

The Niobrara Formation is one of only two Cretaceous intervals rich in

carbonate sediments in the Rocky Mountain region (Longman, 1998). The high

organic content found in this interval may serve as a source for its hydrocarbon

potential.

Late Cretaceous
85Ma

Figure 2 - Late Cretaceous time during the deposition of Niobrara Shale. This figure
shows the extent of the Western Interior Seaway. It should be noted that a mountain
range lies just to the west of the seaway, which is the source for the various types of
siliciclastics and shales deposited in the area during this time (Blakey, 2011).

First proposed by Scott and Cobban (1964), the Niobrara Formation is composed

of the underlying Fort Hays limestone Limestone and the Smoky Hill Shale

member above (Fig. 4), various researchers over the past three decades

(Kauffman, 1969; 1977; Hattin, 1981; Barlow and Kauffman, 1985) have agreed

with this classification. As a ledge-forming unit composed largely of multiple

layers of gray hard limestone, the Fort Hays limestone has a thickness of

approximately 40 ft (Scott and Cobban, 1964). The 700 ft of Smoky Hill Shale

contains seven units; four limestones making up the lower portion while the upper

portion is composed of alternating layers of sandy shales and chalks (Scott and

Cobban, 1964).
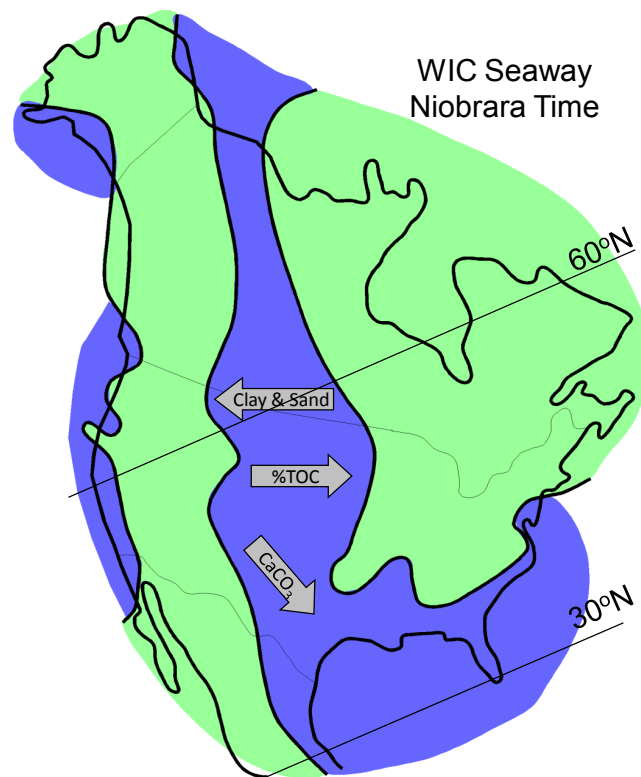
Figure 3 - Western Interior WIC? Seaway illustrating regional depositional trends during the deposition of the Upper Cretaceous Niobrara (Sonnenberg, 2012).
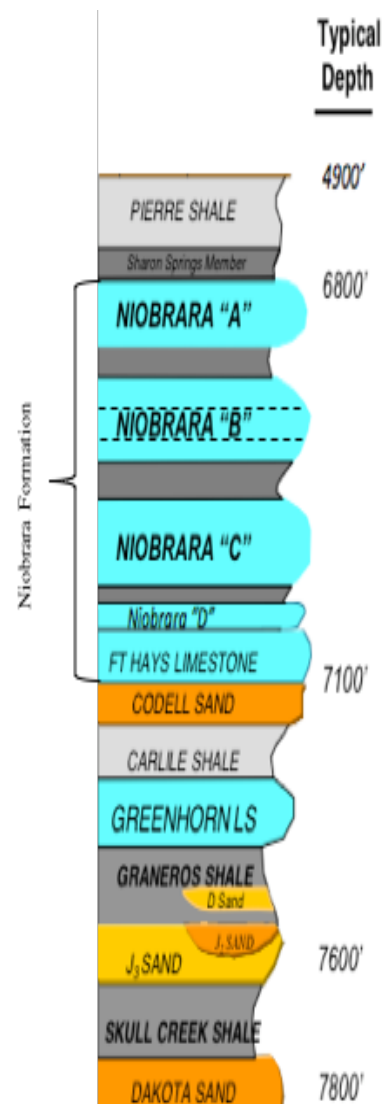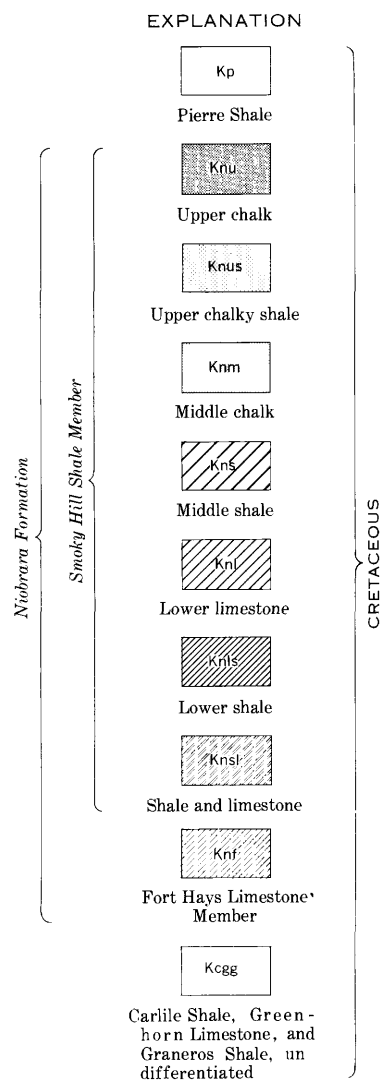
Figure 4 - Stratigraphy of the Niobrara Shale, first proposed by Scott & Cobban (1964), is made up of approximately 700 ft of the Smoky Hill Shale Member and 40 ft of Fort Hays Limestone.

Figure 5 - Expanded stratigraphy proposed by Longman(1998), which includes 10 stratigraphic sections within the Niobrara Formation including the previously unclassified "D" bench (modified from Sonnenberg, 2012).

More recently, with an elaboration of the original classification by Scott

and Cobban (1964), Longman (1998) has classified four, expanded from three,

major chalk benches (A-D) separated by intervening shale beds within the

Smokey Hill Member of the Niobrara (Fig. 5). This new and accepted

classification has increased the number of benches within the Niobrara to 10;

these intervals include the Fort Hays Limestone at the base of the Niobrara, and

nine chalky-marly-shaly intervals within the Smoky Hill Member (Longman, 1998;

Luneau et al, 2011; Sonnenberg, 2012). The type log shows a distinct gamma ray

signature for each interval within the Niobrara and shows the previously

unclassified N850 interval which directly overlies the Fort Hays Limestone (Fig. 6)

(Longman, 1998). Longman (1998) classified the N850 interval as the "D" chalk

or basal chalk. The Niobrara Formation unconformably lies above the Carlile

Shale below, and is capped by the carbonate poor Pierre Shale above (Locklair,

2007). Deformation during the Laramide has caused the Formation to be highly

faulted and contains low-relief structures potentially trapping valuable

hydrocarbons which are sealed by the Pierre Shale above (Brown et al., 1982).

The highly brittle nature of the Niobrara Formation makes it susceptible to

tension faulting, forming horsts and grabens which have historically served as

stratigraphic oil traps.

TYPE LOG

Andrau Enterprises #13 Owl Creek
NW NW Sec. 29 T7N R64W
Weld County, CO
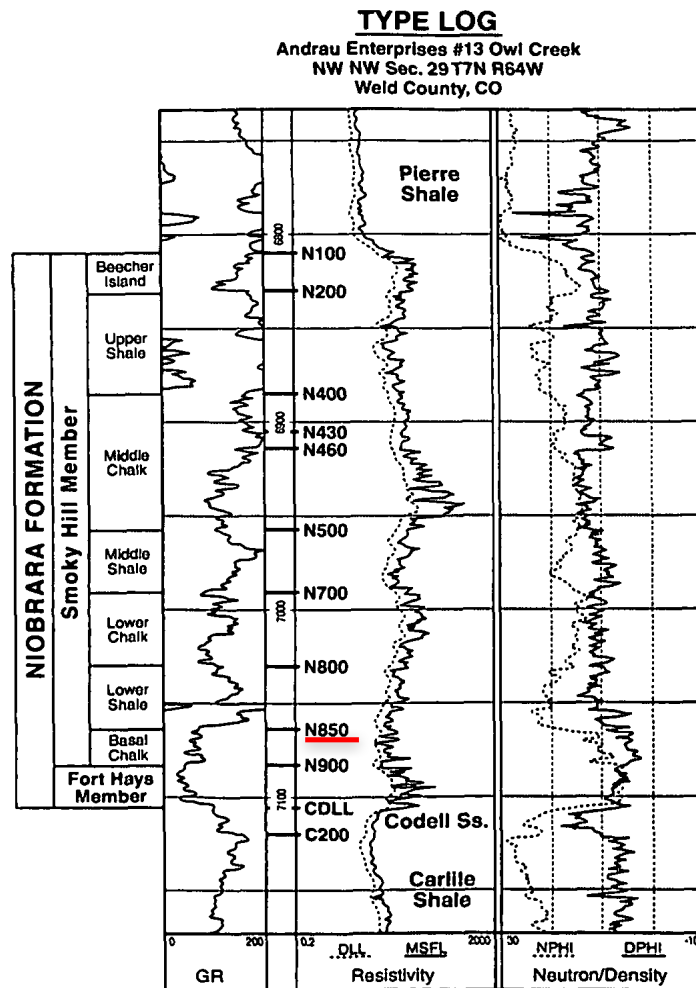
Figure 6 – Type log which shows individual gamma ray signatures for various benches within the Niobrara Formation (Longman, 1998).

Petroleum Potential

In 1919, the Midfields No. 1 well was drilled in Yuma County, Colorado which turned out to be a discovery well for the Beecher Island Field (Brown, 1982). Gas flow rates for the Midfields No. 1 well were estimated at 2MMcf/D, subsequently 4 additional wells were drilled into the Niobrara (Brown, 1982). In

3

light of their limited success, two of the four wells were drilled into deeper formations, which curiously had gas shows as they were penetrating the Niobrara. Additional wells were drilled into the Niobrara, but they soon proved to be uneconomic with an average production of 20Mcf/D (Brown, 1982). Despite their shortcoming, the Midfield well proved the existence of significant reserves within the Niobrara.

In the Denver Basin of Eastern Colorado, the Niobrara has been classified as a calcareous dolomitic mudstone composed largely of chalks and limestones (Brown, 1982; Longman, 1998; Thomas, 2005). Production from various lithologies in the Niobrara changes dramatically over the expanse of the Formation from East to West. Production in the Eastern section comes from microporous and fractured coccolith and planktonic foraminifer-rich limestones, and the Western portion sees production from fractured sand-rich facies, while the Central region attributes production to fractured marls and shales (Longman, 1998). Sonnenberg (2012) compared the Niobrara to the Eagle Ford Shale in South Texas, which was deposited during the same time period and has an estimated 5.1 BBOE in reserves (EIA, 2015).

Hypothesis

In this work, I argue that mineralogical controls are responsible for the porse size distribution and porosity seen in unconventional reservoirs, such as

the Niobrara Formation. This work specifically examines the relationship of various geological controls (TOC and mineralogy) on pore size distribution from MICP and low-pressure nitrogen sorption tests, as well as pore connectivity from wettability and imbibition tests.
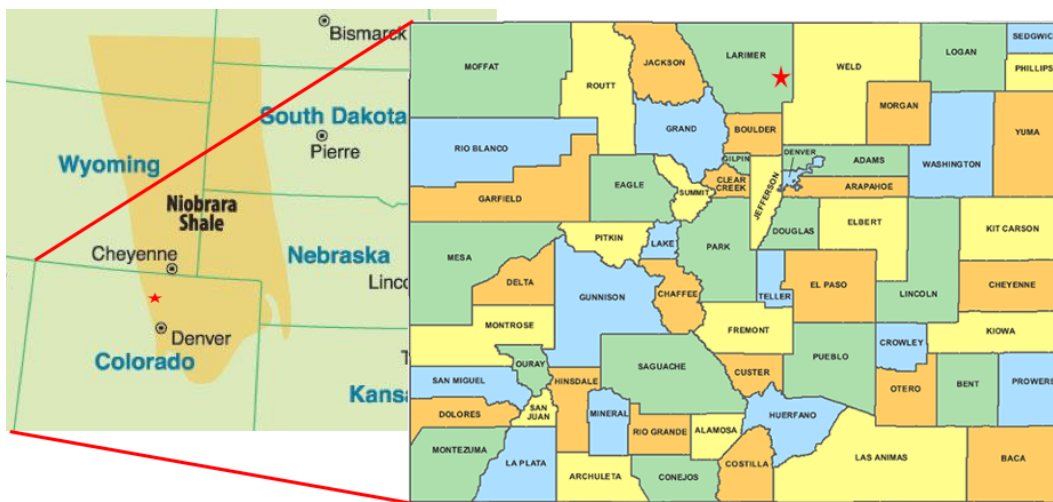
Figure 7 - Well location (depicted by a red star) of Berthoud State #3 and close-by Berthoud State #4 in Larimer County, Colorado (modified from digital-topo-maps.com, 2005; Fessler, 2011).

Well Name	API #	County	Location (Latatude and Longitude)	Operator	Measured Depth (ft)
Berthoud State #3	506906054	Larimer	40.309424, -105.124292	Coquina Oil	2910-3185

Table 2-1 Berthoud State #3 well location and operator obtained from USGS core repository.

Gamma Ray

"B Chalk" — N400

"B Marl" — N430

N460

N500

"C Chalk" — N700

"C Marl" — N800

"D Chalk" — N850

Fort Hays

Codell SS

0   200
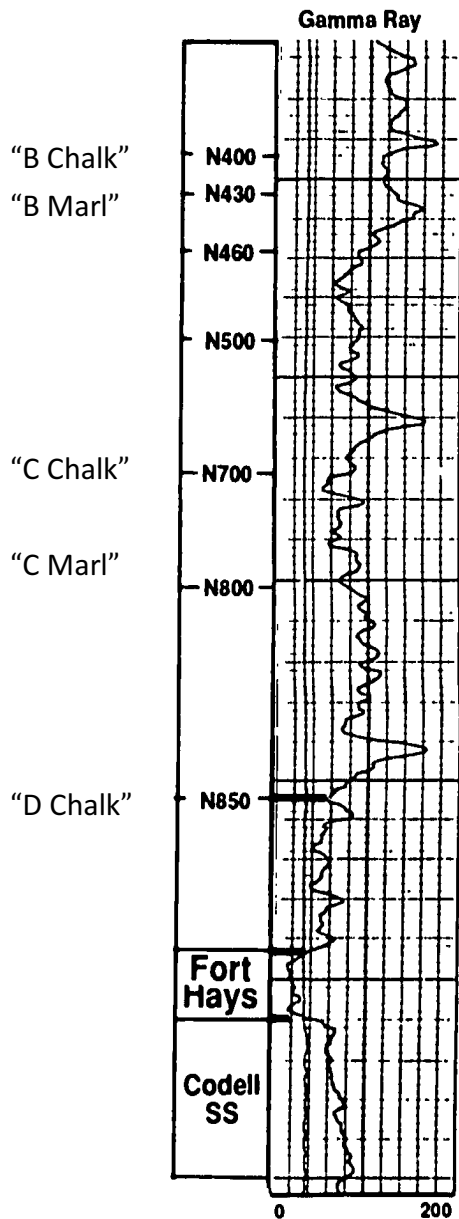
Figure 8– Gama ray signature showing multiple benches in the Berthoud State #3 well of interest (modified from Longman 1998.

The Niobrara Formation is composed of multiple layers of gray limestone, with alternating layers of chalks and sandy shales high in organic content (Scott and Cobban 1964). Longman (1998) identified a total of 10 benches which form the Niobrara Formation. The formation varies in thickness throughout its expanse, but has an average thickness of 700 ft (Scott and Cobban, 1964). Core samples were allocated from the USGS Core Repository in Denver, Colorado. Berthoud State #3 well was selected for study based upon its inclusion of all benches within the Niobrara (Fig. 7; Table 3-1); in addition, the sandstone below Niobrara Formation is also included as a comparison. Previous work, conducted by Longman (1998), was utilized to select the depth of desired benches within the slabbed core (Fig. 8). Two

mini plugs, a total of 14 samples, were taken from each bench within the core in order to conduct various tests on the Formation. Each sample was then cut into 1cm cubes for laboratory tests and assigned a laboratory identification (Table 3-2).

Berthoud State #3			
Bench	Lab Identification	Lithology	Depth (ft)
A	CO B129A	Chalk	2925
AM	CO B129AM	Marl	2988
B	CO B129B	Chalk	3039
BM	CO B129BM	Marl	3060
C	CO B129C	Chalk	3074
CM	CO B129CM	Marl	3107
D	CO B129D	Chalk	3166
Fort Hayes Limestone	CO B129 FHLS	Limestone	3194
Colorado Sandstone	CO B129 CSS	Sandstone	3210

Table 3-1 - Laboratory identification, lithology, and depth of samples obtained from Berthoud State #3 well.

Methods

In order to holistically quantify pore size distribution and pore connectivity of the selected samples, several tests (XRD, wettability, mercury injection capillary pressure, low-pressure gas sorption, imbibition) have been performed, and the results are discussed with respect to geological characteristics (e.g., TOC, mineralogy).

Wettability

Wettability tests determine the wetting characteristics (whether or not the sample is wetting or non-wetting to a fluid) of the shale samples to n-decane and API brine, which exhibit an affinity for the organic matter phase or mineral phase respectively. Due to the limitation of sample mass, thin (~ several mm) sample fragments were utilized for this experiment unlike other tests which relied on cubic samples. The DinoXcope was used to photograph the samples before and after adding 2 µL of one fluid (eiter *n*-decane or API brine). Opposite sides of the same sample were then utilized for another fluid*,* and samples were discarded after use.

Video was taken while pipetting 2 µL of the aforementioned fluids to record their spreading characteristics on the shale samples. The spreading of the fluids was recorded for approximately 30 seconds, or until the spreading reached the edge of the sample or progression of the spreading ceased. A number between 1 and 10 was assigned to describe the spreading behavior observed during the wettability test in an attempt to qualitatively assess the wetting characteristics of the sample. Samples with seemingly little to no spreading of the solution were classified with the lowest number (1), where as samples with immediate or very rapid spreading were characterized with higher values.

Powder XRD (x-ray diffraction) analysis is performed to collect mineralogy information of the Niobrara samples of different benches. Representative core samples were disaggregated, micronized in a McCrone Mill, mounted, and scanned with a Rigaku Ultima IV XRD (Cu tube, monochromator, scintillation detector) at the University of Oklahoma. Quantitative mineralogy is determined by whole-pattern fitting in Jade2010 using the MDI-500 and ICDD PDF-4+ databases. Following air drying, glycolation, and heat treatment, clay mineralogy is determined by preparing and scanning oriented filter peel mounts(Madden et al., 2006).

Mercury Injection Capillary Pressure (MICP)

Porosity, pore-size distribution, permeability, and tortuosity can be analyzed by utilizing the mercury injection capillary pressure (Micromeritics AutoPore IV 9510) available at the Univeristy of Texas at Arlington (Fig. 9). In order to determine the aforementioned properties of a rock sample, the AutoPore IV9510 produces pressures incrementally up to 60,000 psia forcing mercury into the pore throats. According to the Washburn (1921) equation, these pressures allow mercury to invade into a pore throat diameter down to 2.8nm. This instrument also has the ability to perform low-pressure analysis that allows the examination of larger pores on the order of 300 µm. From raw data

of pressure and intruded volume used to calculate densities, pore volume, and

pore throat size, mercury injection capillary pressure (MICP) has the ability to

analyze other pore characteristics such as total pore surface area, permeability,

and tortuosity (Micrometrics, 2011; Hu and Ewing, 2014).

Mercury is a non-wetting substance which does not naturally invade

pores unless an external pressure is applied. Washburn (1921) devised an

equation which states that the diameter of pore-throats invaded by mercury are

inversely proportional to the pressures applied; the higher the pressures used to

force mercury into the pore throats, the smaller the pores. This can be

expressed by the equation developed by Washburn (1921) which is based on the

premise that all pores are cylindrical in shape.

$$\Delta P = -\left(\frac{2\gamma cos\theta}{R}\right)\ldots\ldots\ldots\ldots(3.1)$$

where ΔP is the pressure difference across the curved mercury interface; γ is the

surface tension of mercury; θ is the contact angle between mercury and the

porous medium; R is the corresponding pore-throat radius. Using γ = 485

dynes/cm and θ = 130°, Equation 3.1 becomes:

$$\Delta P = \frac{90.43}{R}\ldots\ldots\ldots\ldots(3.2)$$

with ΔP in psia and R in micrometers (μm) (Hu and Ewing, 2014).

More recently Wang et al. (2016) suggested that the contact angle of mercury in a circular pore increses exponentially as pore size decreases, this becomes especially important with pores that have a radius of smaller than 5 nm such as those seen in tight shale formations. In order to account for the variability in these properties, the once constant liquid-vapor surface tension of mercury and contact angle measurements (Υ and θ respectively) are represented by

$$\gamma(r_c) = \gamma_\infty \left(1 - \frac{1}{4r_c/h-1}\right) exp \left(-\frac{2S_b}{3R}\frac{1}{4r_c/h-1}\right) \dots\dots\dots(3.3)$$

$$and$$

$$\theta_{Hg} = \theta_{Hg\infty} + C_1 exp \left(-\frac{r-C_2}{C_3}\right) \dots\dots\dots(3.4)$$

where, r_c is droplet radius, $S_b = E_0 / T_b$ and E_0 is the enthalpy of vaporization (kJ/ml); T_b is the boiling point (K); R is the ideal gas constant; and h is the effective atomic or molecular diameter(nm) (Wang et al., 2016).

The equation proposed by Wang et al. (2016) correlates the mercury intrusion capillary pressure to the pore radius and combines variable contact angle measurements as well as taking into account the changes in surface tension of mercury and can be represented by

$$P_c = -\frac{2\gamma_{Hg}(r)\cdot\cos\theta_{Hg}(r)}{r} \dots\dots\dots(3.5)$$

with comparison to the original Equation 3.1 devised by Washburn (1921), γ_{Hg} and θ_{Hg} are functions of r instead of remaining constant.

Throughout the testing procedure, MICP records intruded volumes associated with pore throats (from applied pressures) that are both invadable by mercury at specific pressure and connected to the mercury reservoir surrounding the sample (Hu et. al, 2014). Despite MICP being one of the most widely accepted approaches to determining pore-throat distribution, the ink-bottle phenomenon, whereby smaller pore throats connect to larger pores, may cause this technique to underestimate the volume of large pores and overestimate that of small pores (Hu and Ewing, 2014; Kauffman, 2010). Furthermore, pores are rarely cylindrical in real world applications. Despite
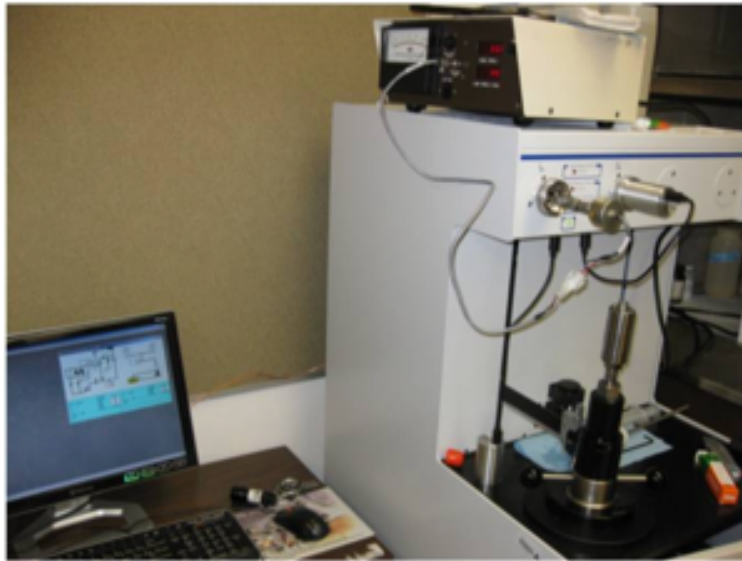

Figure 9 - Micromeritics AutoPore IV 9510 used for both low and high pressure analyses.

some shortcomings, this methodology has proven to be more than satisfactory for

the majority of applications.

Porosity, median pore-throat diameter, and permeability of the samples

can also be calculated as reported by Gao and Hu (2013) through the use of

methodology outlined by Katz and Thompson (1986; 1987) and tortuosity by

Hager (1998) and Webb(2001). Katz and Thompson (1986; 1987) applied the

following equation to determine the permeability of samples by utilizing

pressure and intrusion volume measurements from MICP data:

$$k = \left(\frac{1}{89}\right)(L_{max})^2 \left(\frac{L_{max}}{L_c}\right) \Phi S(L_{max}) \ldots\ldots\ldots\ldots(3.6)$$

where k is the air permeability (μm^2); L_{max} is pore throat diameter when

hydraulic conductance is at a maximum (μm); L_c is the length of the pore throat

diameter (μm) corresponding to the threshold pressure obtained from the

inflection point of the cumulative intrusion curve P_t (psia); Φ is porosity; $S(L_{max})$

denotes the fraction of connected pore space composed of pore width of size

(L_{max}) and larger (Gao and Hu, 2012).

Pore connectivity can also be related to effective tortuosity, τ, and can be

derived from MICP data (Hu et al., 2015).

$$\tau = \sqrt{\frac{\rho}{24k(1+\rho V_{tot})} \int_{\eta=r_{c,min}}^{\eta=r_{c,max}} n^2 f v(\eta) d\eta} \ldots\ldots\ldots\ldots.(3.7)$$

where ρ is fluid density (g/cm^3); V_{tot} is total pore volume, mL/g;

$\int_{\eta=r_{c,min}}^{\eta=r_{c,max}} n^2 fv(\eta)d\eta$ is pore throat volume distribution by pore throat size (Hu

et al., 2015).

Procedure

Individual shale samples were first cut into cubes of approximately 1cm x

1cm x 1cm in length and oven dried at 60°C for a minimum of 48 hours in order

to remove any moisture which may have been trapped within individual pores.

Before the MICP procedure began, samples were removed from the oven and

allowed to cool to room temperature (approximately 23° C) in a desiccator with

less than 10% relative humidity. The desiccator was used to minimize additional

moisture intrusion into the sample before MICP analysis.

To begin MICP analysis a sample of one cube (2-3 grams) was placed in its

corresponding potentiometer, which consists of a sample bowl connected to a

precision metal and glass capillary system. The potentiometer is then sealed

with the sample inside and placed in the low pressure chamber where the

sample is evacuated to 50 μm Hg (0.05 torr, 0.000972 psi, 6.7 pa). This process

removes any excess air and moisture which may still be present within the

sample.

Each sample undergoes both low pressure and high pressure analyses

during an MICP test. Low pressure analysis with shale samples fills the sample

chamber with mercury to a maximum of 30 psia utilizing an equilibrium time of 10 seconds to achieve a stable mercury level before proceeding to higher pressure intrusion. During low pressure analysis, mercury initially invades pores which it can easily access by overcoming capillary pressure of larger pore throats with a limit of 300µm (Chukwuma, 2015). High pressure analysis incrementally increases pressure from 30 psia up to 60,000 psia at an equilibrium time of 45 seconds between pressures, allowing mercury to intrude pore throats as small as 2.8 nm (Hu and Gao, 2012). Throughout the MICP testing procedure, the volume of mercury intruding the sample is recorded with it's corresponding pressure. Utilizing this in conjunction with mercury's surface tension and contact angle between shale samples, values for porosity, pore throat radius, permeability and tortuosity can be obtained (Gao and Hu, 2012; Hu and Ewing, 2014; Chukwuma, 2015)

<div align="center">Low-pressure gas sorption</div>

Low-pressure nitrogen sorption isotherm tests use Niobrara samples at the size fraction of mesh 35/20 (e.g., 500-850 um) with QuadraSorb™ SI Surface Area and Pore Size Analyzer (Quantachrome Instruments) at Chengdu University of Technology in China. A dried sample weighing approximately 1 g was placed into the sample cell, with a tube inner diameter of 9 mm, which is installed onto the sample degassing apparatus and evacuated at 80°C for 12 hours. A tank of

liquid nitrogen (77.3 K) was placed around the sample tube for the isotherm test. The nitrogen gas is dosed, and allowed to adsorb, onto the sample. The quantity adsorbed under different relative pressures of nitrogen is recoded, giving gas adsorption isotherms, and the surface area of samples is obtained from the gas adsorption isotherms according to the BET (Brunauer, Emmett and Teller) equation (Brunauer et al., 1938) with a multi-point approach. Pore size distribution is obtained by BJH (Barrett-Joyner-Halenda; Barrett et al., 1951) method for the measurement range of 3.1-220 nm and DFT (density functional theory) for 1.41-36.0 nm (Ravikovitch et al., 1998).

<center>Fluid Imbibition and Tracer Migration</center>

Imbibition is known as a process whereby a wetting fluid displaces a non-wetting fluid on the basis of capillary suction alone (Hu et al, 2014). Fluid imbibition can be conducted in one of two ways; forced, which involves the use of an external pressure to promote the uptake of a fluid, or spontaneous, if the sample is placed in a fluid and fluid uptake is due solely to a wettability difference and capillary forces within the porous media (Morrow et al, 2001; Lopez and Soria, 2007). In addition to illustrating pore connectivity of a rock sample, imbibition data can also be correlated with variations in permeability, porosity, boundary conditions and liquid viscosity ratios (Morrow et al, 2001). Predominantly a capillary controlled process, spontaneous imbibition rate

<center>16</center>

depends upon the properties of the porous media, fluid which is being imbibed, and the fluid-rock interaction (Morrow et al., 2001). Two fluids (DI water and decane) were used for the imbibition process during this study of the Niobrara Formation (Fig. 10). Imbibition within the Niobrara Formation provides not only a better understanding of pore connectivity within the rock, but also provides insight into the reservoir quality of the formation.

Imbibition provides a cost-effective way of understanding pore connectivity for a given rock sample, due to a mathematical analogy between diffusion and imbibition (Hu et al., 2012; 2014). Ewing and Horton (2002) utilized a network model based on percolation theory to estimate pore connectivity, which examined the slope of the log of imbibed liquid mass versus log imbibition time (Hu et al., 2012; 2014). This approach qualitatively determines a rock's pore connectivity and may be expressed as a slope of ¼, ¼ changing to ½, or ½ (Hu et al., 2012; 2014). Further details regarding the use of percolation theory can be found in Stauffer and Aharony (1994), Ewing and Horton (2002) and Hu et al. (2012).
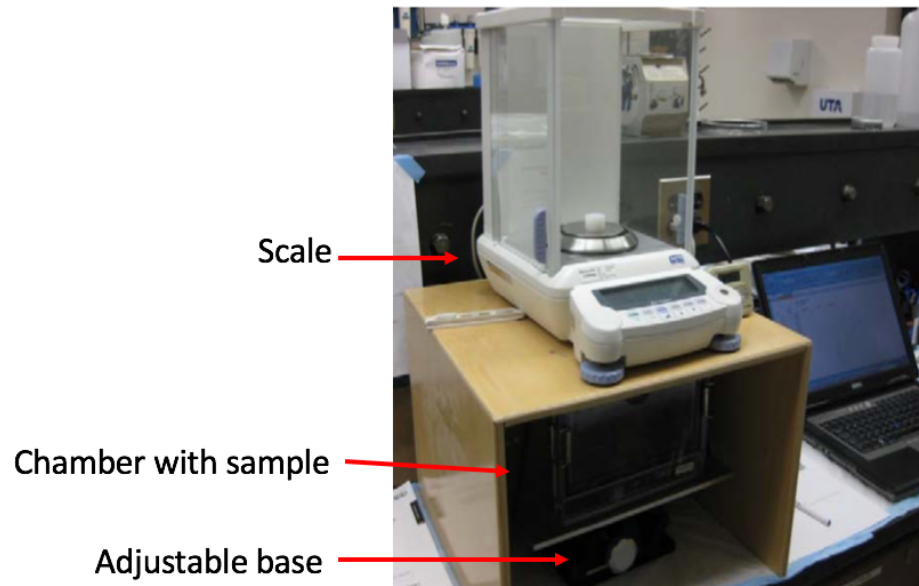
Figure 10 – Imbibition apparatus used for fluid imbibition utilizing DI, *n*-decane, and brine (modified from Hu et al., 2014).

Oil and gas recovery is highly dependent upon the spontaneous imbibition process because oil and gas is displaced by water within a fractured matrix (Hu and Ewing, 2014). Extensive research has been conducted to further investigate the correlation between imbibition and oil/gas production (Li, 2007; Standnes, 2010; Hu and Ewing, 2014).

Procedure

Cubic samples were epoxied on all sides except for the top and bottom. The use of epoxy on the sample surfaces served two purposes: 1) to avoid evaporation of the imbibing fluid from the sides of the sample; 2) to allow for imbibition up the external surface for the study of 2-D migration along the sides.

Before starting the imbibition process could begin, samples were oven dried at 60ºC for a minimum of 48 hours, which ensured a consistent initial water saturation state. For DI water and API brine imbibition tests, beakers of water were placed inside the experiment chamber in order to maintain a relatively constant humidity level, minimizing fluid evaporation from the fluid reservoir. The top and sides of the sample were loosely covered with aluminum foil, leaving a small hole for air to escape, before being placed into the imbibition apparatus which can be seen in Figure 9. The aluminum foil reduced vapor transport and capillary condensation on the top face of the sample. The bottom of the sample was then submerged to a depth of approximately 1mm into the fluid reservoir exposing only one side of the sample to a fluid composed of either DI water, brine or *n*-decane (with and without tracers). Imbibition rate was obtained from automatic recording of sample weight change over time.

Tests which utilized brine or *n*-decane with tracers were stopped after 24 hours, frozen in liquid nitrogen, freeze dried, and stored at < 10% relative humidity before being mapped for tracer distribution utilizing laser ablation coupled with inductively mass spectrometry (LA-ICP-MS) (Hu, 2014). LA-ICP-MS used a 100 μm spot diameter UP-213 laser in order to vaporize a hole in the shale sample at submicron depth; elements which were entrapped within the pore structure were consequently vaporized and analyzed with ICP-MS (Hu,

2014). Utilizing LA-ICP-MS allowed for 2-D mapping to be performed on the

chemical distribution of the various shale samples (Hu & Mao, 2013).

Chapter 4 Results and Discussion

Mercury Injection Capillary Pressure (MICP)

Through the use of the methodology outlined by Hu (2014), MICP testing

is able to utilize the pressure at which mercury invaded the shale samples to

estimate the pore-throat size distribution. In addition, MICP testing is able to

determine other petrophysical properties such as bulk density, porosity,

permeability, and tortuosity.

All of the Niobrara samples tested had an average pore size of 0.0028 μm

− 0.05 μm, with only a small portion, less than 3% by volume, exhibiting pore

sizes greater than 0.1 μm (up to 36 μm), with the exception of the Fort Hays
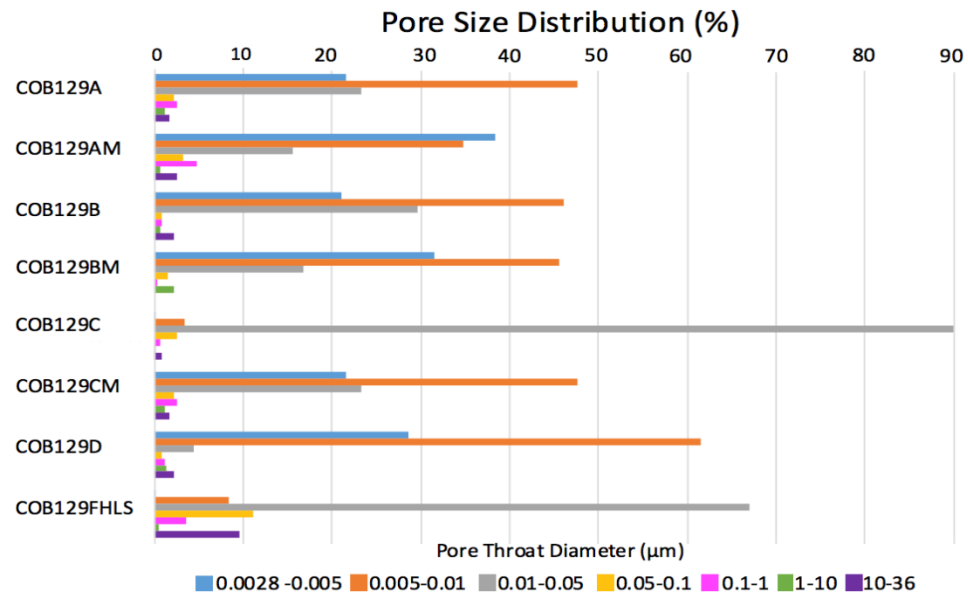
Limestone (Fig. 11, Table 4-1).

Figure 11 – Pore-throat size distribution of Niobrara Formation in Berthoud State #3 well.

Sample ID	Pore Size (μm)						
	0028-0.005	.005-0.01	0.01-0.05	0.05-0.1	0.1-1	1 - 10	10 - 36
COB129A	21.6	47.7	23.4	2.12	2.51	1.12	1.63
COB129AM	38.5	34.8	15.6	3.14	4.75	0.684	2.60
COB129B	21.0	46.0	29.6	0.752	0.856	0.618	2.19
COB129BM	31.5	45.6	16.8	1.47	2.58	2.25	0
COB129C	0.17	3.43	92.3	2.46	0.686	0.103	0.831
COB129CM	21.6	47.7	23.4	2.12	2.51	1.12	1.63
COB129D	28.5	61.5	4.41	0.822	1.08	1.42	2.22
COB129FHLS	0.034	8.37	67.1	11.1	3.49	0.464	9.51
COB129CSS	4.36	4.07	26.8	22.9	34.7	0.944	6.33

Table 4-1 – Pore-throat size distribution (%) results from MICP.

By individually comparing the chalk/shale (A-D in sample ID) and marl

(ending with M) samples, it became apparent the chalk benches typically

exhibited a larger pore throat size in the range of 0.005μm – 0.05μm in

comparison to the marls which generally had a pore throat size of 0.0028 –

0.01μm (Figs 12-13; Table 4-1). Nearly 66-75% of pore throats from chalk

samples COB129A, COB129B, and COB129D were represented by pores in the

range of 0.005 μm-0.01 μm, while 92% of pores from COB129C were in the size

of 0.01 μm-0.05 μm (Fig. 12). Pore throats between 0.0028 – 0.05 μm

accounted for 92-96% of all pores within chalk samples. All three marl samples

tested had roughly 60-70% of pores ranging in size from 0.0028 – 0.01 μm, with

samples CO B129BM and CO B129CM having nearly 46% and 48% of their pores

between 0.005 – 0.01 μm respectively (Fig. 13). Marl samples showed nearly

90% or greater pore throat sizes between 0.0028 – 0.05 μm. Other

petrophysical properties investigated through MICP tests determined porosity,

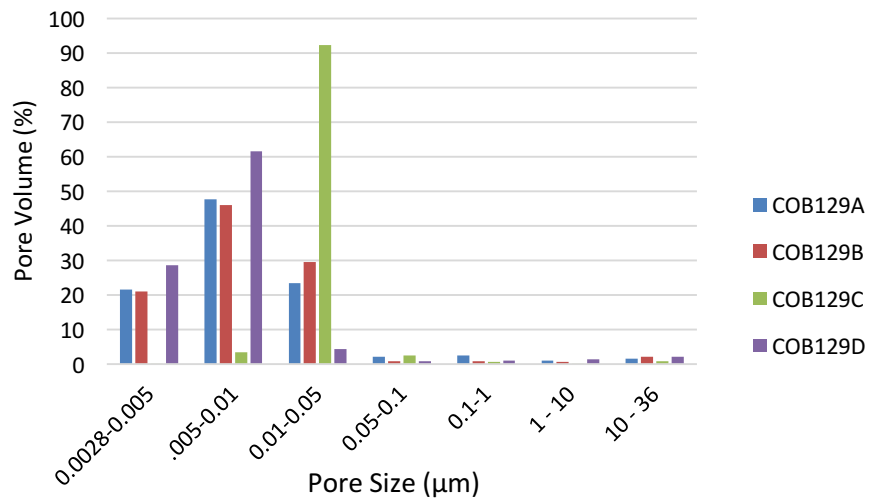bulk density, tortusoity, and gives clues as to matrix permeability (Table 4-2).

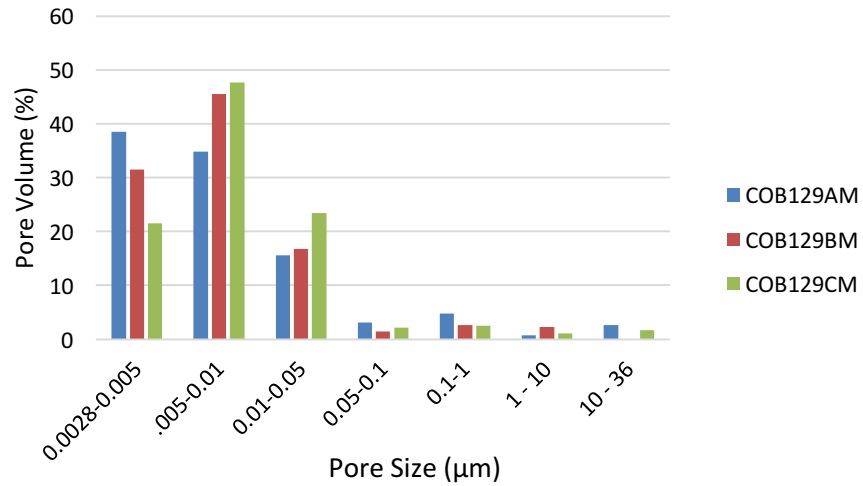Figure 12 - Pore-throat size distribution of chalks tested through MICP.

Figure 13 - Pore size distribution of marls tested through MICP.

Sample ID	Sample dimension	Sample mass used (g)	Total pore volume (cm^3/g)	Total pore area (m²/g)	Median pore-throat diameter D_{50} (Volume)	Median pore-throat diameter (Area) (nm)	Median pore-throat diameter (4V/A) (nm)	Bulk density (g/cm^3)	Apparent (skeletal) density (g/cm3)	Porosity (%)	Have pores less than 3 nm (yes/no)	Geometric mean for k (m2)	Harmonic mean for k (m2)	"Tortuosity" (D0/De)	Le/L [square root of (tortuosity *porosity)]
CO B 129A	2 fragments	2.22	0.036	4.4	33.8	33.8	31.4	2.42	2.64	8.38	no	1.39E-20	8.21E-21	3929	13.14
CO B 129AM	2 fragments	2.48	0.008	6.1	5.0	4.0	5.4	2.50	2.55	2.05	no	3.21E-21	2.00E-21	2480	6.30
CO B 129B	2 fragments	2.08	0.018	11.6	6.3	5.1	6.2	2.48	2.59	4.47	no	2.83E-20	1.11E-20	1697	8.54
CO B 129 BM	2 fragments	2.01	0.011	7.7	5.2	4.5	5.5	2.51	2.58	2.67	yes	5.14E-21	3.94E-21	0	0.0
CO B 129 C	2 fragments	2.79	0.026	6.6	18.3	18.3	15.9	2.46	2.64	6.48	no	3.32E-02	4.16E-19	918	7.71
CO B 129 CM	2 fragments	2.43	0.018	11.5	6.0	5.0	6.2	2.45	2.56	4.36	yes	3.13E-20	1.38E-20	1666	8.31
COB129 D	1-cm cube	2.28	0.019	11.6	6.4	5.4	6.5	2.53	2.66	4.79	yes	3.11E-17	3.47E-20	711	4.36
COB129 FHLS	1cm cube	2.12	0.028	5.3	29.3	17.0	21.4	2.47	2.65	7.01	no	1.67E-16	2.20E-18	12367	29.24
COB129 CSS	1cm cube	1.74	0.056	7.6	72.7	7.2	29.4	2.25	2.57	12.56	no	NA	NA	15543	42.97

Table 4-2 – Petrophysical results obtained through MICP for Berthoud State #3 well

When comparing the composition of chalks/shales and marls within the Niobrara to the pore throat sizes, it became apparent the mineralogical composition played an intrinsic role. For chalk-rich samples, benches A, B, and C exhibited a higher calcite content, as well as lower illite and quartz contents. Found to be in the range of 5 – 50 nm, the pore throat sizes of these samples were generally larger than the marl samples. In contrast to the chalk samples, the marl samples (AM, BM, and CM) all possessed a lower calcite content but a higher clay and quartz content. This will be further elaborated upon in Discussion section.

Wettability

API brine, DI water, isopropyl alcohol (10% in water v/v), and *n*-decane were used during wettability tests (Fig. 12; Table 4-3). Dispensing each of these fluids and observing either the hydrophilic or hydrophobic characteristics helps determine the wetting behavior of the sample. During the testing procedure it was noted that samples which exhibited low spreading behavior with API brine or DI water had high spreading characteristics with *n*-decane. This phenomenon is most likely due to the affinity of *n*-decane to the kerogen or organic matter phase (which is microns in size and dispersed throughout the sample) and the affinity towards the mineral phase for API brine.

When 2µl of API brine, DI water, or 10% IPA was applied to the various chalk and marl samples, the solution typically formed a bead on the surface with a high mineral/air contact line, indicating the samples being oil-wet (Borysenko et al., 2009). Despite most samples exhibiting similar wetting characteristics between three fluids, there were some notable differences. Sample CO B129 C had a spreading value of 2 with DI water yet API brine (with much higher salinity than DI water) produced a result of 6 for moderate spreading. In addition, CO B129 CM produced a spreading value of 5 with DI water and had a value of 1 for API brine forming a bead on the sample surface.

Similar to the process of applying API brine, applying 2µl of *n*-decane on the same benches showed the samples' surfaces were hydrophobic. Conversely to the high contact angle seen when using API brine, the affinity for *n*-decane exhibited by the samples produced a low contact angles and in most cases were adsorbed into the sample almost instantaneously. These findings further affirmed the results found when using API brine. The hydrophobic nature of the shale samples towards API brine, DI water, and 10% IPA and hydrophilic affinity towards *n* –decane suggests that the samples are oil-wet source rocks.

Sample ID	Wettability Scale			
	DI Water	API Brine	*N* - decane	IPA 10%
CO B129A	1	1	10	1
CO B129AM	3	3	10	4
CO B129B	3	5	10	2
CO B129BM	5	5	10	5
CO B129C	2	6	10	4
CO B129CM	5	1	8	4
CO B129D	6	7	10	7
CO B129FHLS	7	8	9	7
CO B129CSS	9	8	10	9

Table 4-3–Wettability test results. All of the Niobrara marl and chalk samples had values below 7 for API brine, DI water and 10% IPA, but above 8 for *n* – decane.
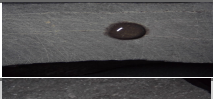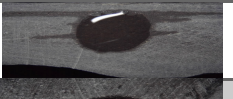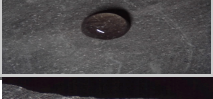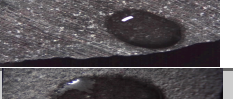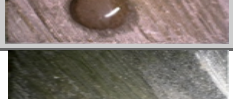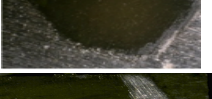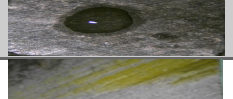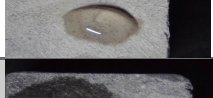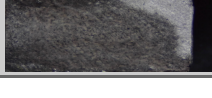
Sample ID	DI Water	Api Brine	N-decane	IPA (10%)
CO B129 A				
CO B129 AM				
CO B129 B				
CO B129 BM				
CO B129 C				
CO B129 CM				
CO B129 D				
CO B129 FHLS				
CO B129 CSS				

Figure 14 - Droplet wettability test results utilizing four fluids.

XRD Analysis

The quantitave mineralogy (wt%) of all benches studied within the Berthoud State #3 well are depicted by

Table 4-4. The samples are predominantly composed of calcite and clay minerals, in addition to some siliciclastic

minerals such as quartz (Fig. 15). Calcite composes 58-94% of samples within the Niobrara, while clays within the

various benches, represented by illite, exhibited a weight percentage of 0.5-15.2%. All Niobrara chalk samples had an

illite content of less than 10% while marl samples contained 10.4-15.2%.

Sample ID	Depth	Calcite	Quartz	Illite	Ankerite	Muscovite	Pyrite	Albite	Dolomite	Gypsum	Anorthite	Anhydrite	Fluorapatite	TOC (wt. %)
CO B129A	2925	89.7	5.3	0.5	1.1	1.9	1.5	0.1	0	0	0	0	0	2.2
CO B129AM	2988	66.2	10.4	13.4	0	1.5	4.6	0.2	3.5	0.2	0	0	0	2.9
CO B129B	3039	76.1	11.4	5.4	2.4	0	1.3	0	0	0	3	0.4	0	2.2
CO B129BM	3060	61.6	12.9	15.2	5.7	0	1.6	0	0	0	3	0	0	2.2
CO B129C	3074	91.5	5.8	1.5	0	0	0.7	0	0	0	0.5	0	0	1.4
CO B129CM	3107	75.4	9.3	10.4	0.8	0	0.9	2.3	0	0	0.8	0	0	2.9
CO B129D	3166	58.1	16.6	7.8	2.9	11.3	0.8	0.1	2.4	0	0	0	0	0.9
CO B129FHLS	3194	94.3	3.6	0	0.6	0	0	0	0	1.6	0	0	0	0.1
CO B129CSS	3210	38.3	44.9	5.1	2.9	2	0	5.9	0	0	0	0	0.9	0.7

Table 4-4 – Major mineral composition (wt%) of samples examined within Berhoud State #3 well.
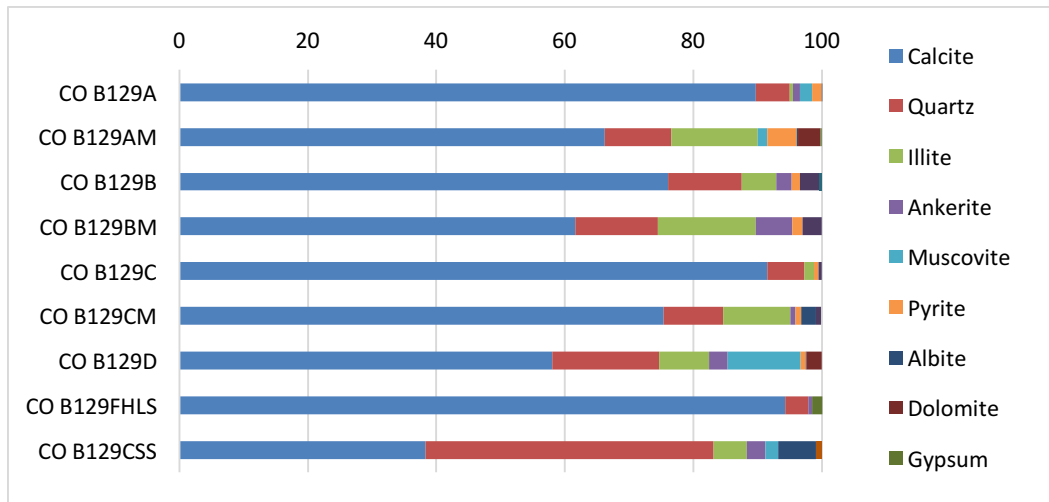
Figure 15 - XRD results from Berthoud State #3 well based on weight percentage

The Niobrara Formation exhibited a strong inverse relationship between calcite and illite weight percentages. When all samples within the Niobrara Formation were examined, an R^2 value of 0.74 was observed suggesting a relatively strong correlation between the two mineral groups (Fig. 16). A more definitive inverse correlation between calcite and illite weight percentages was seen when removing sample CO B129 D, the basal chalk, from the samples (Fig. 17). A duplicate XRD test of CO B129D would affirm current mineralogical results for this sample, as other research suggests the basal chalk has a slightly different composition (Kulia et al., 2012). This strong inverse relationship supports theories that suggest an influx of pelagic chalks during times of warmer climates

and an abundance of shaly chalk units as a result of colder paleo-currents during

the Cretaceous (Longman, 1998).
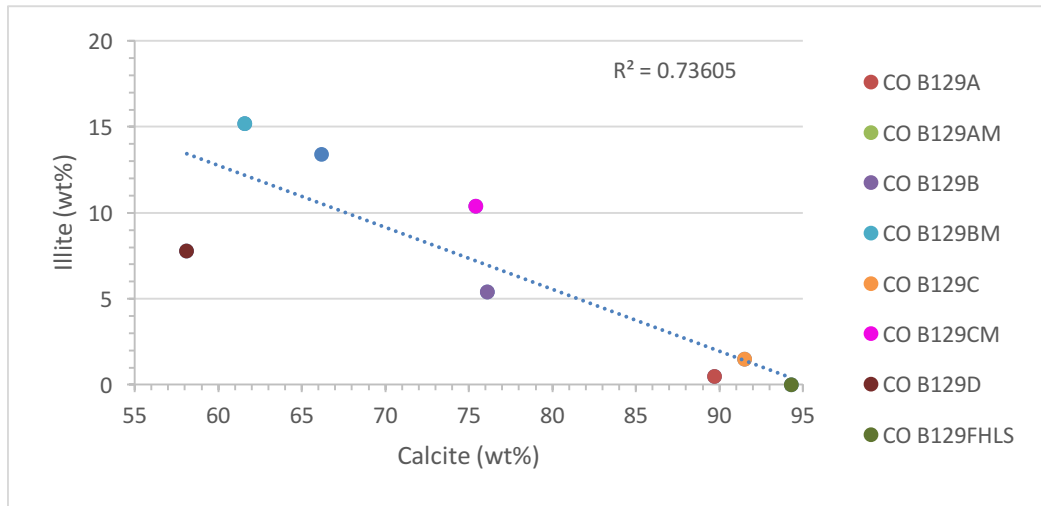
Figure 16 - Inverse relationship between calcite and illite within all Niobrara samples in Berthoud State #3 well. On the same figure, add another line without D sample.
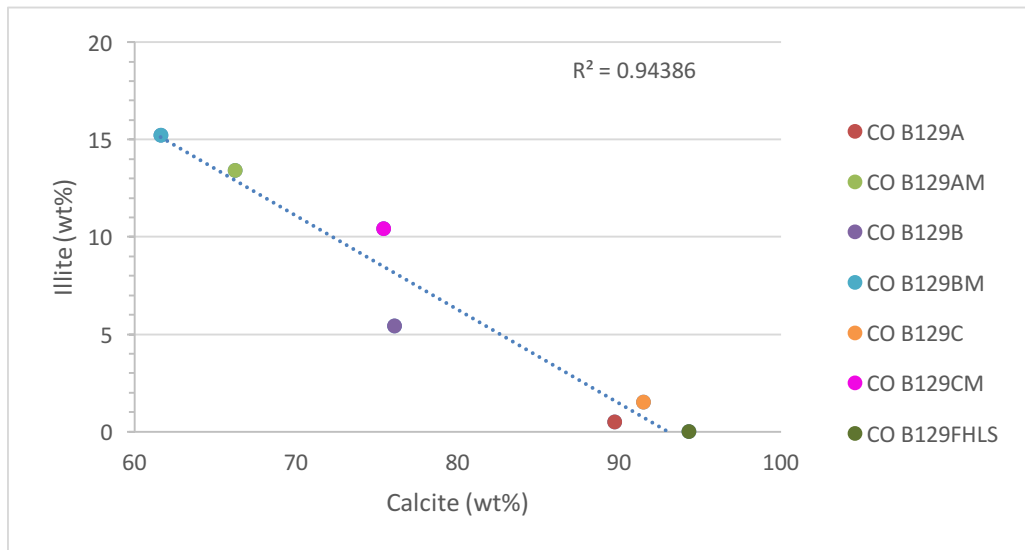
Figure 17 – Inverse relationship, with R^2 value of 0.94386, between calcite and illite with basal chalk CO B129D removed from samples.

Schlumberger's sCore lithofacies classification scheme is a ternary

diagram with three apexes to represent the components clay, carbonate, and

quartz, feldspar and mica (QFM) in weight%. Utilizing a ternary diagram such as

the sCore from Schlumberger allows rocks to be classified based upon their

mineralogy, and potentially linked to well logging and reservoir quality

(Schlumberger, 2014). With the exception of CO B129D, the basal chalk, plotting

samples from the Niobrara Formation on to the sCore lithofacies ternary

diagram showed most lithology's fell into one of two categories (Fig. 18). Chalks

of the Formation are considered a carbonate-dominated lithotype, while marls

are clay-rich carbonate mudstone. Due to the influx of detrital siliciclastic

materials deposited during the formation of CO B129D, the bench is considered

a silica-rich carbonate mudstone and have a different pore structure (Figs.11-12

and 16); such an analysis illustrates the utility of using lithofacies to serve as a

bridge to potentially link pore structure characteristics with other commonly

used reservoir characteristics approaches (e.g., logging).

Basal units of the Niobrara, CO B129D and CO B129FHLS, were thought to

have been deposited under oxidizing conditions with little opportunity for

preservation of organic carbon (Kuila et al., 2012). TOC values of CO B129D and

CO B129FHLS were found to be 0.93 and 0.13 respectively. Sediments from

benches further up section were deposited in deeper anoxic environments which

allowed for greater preservation of organic carbon., and higher TOC values of

1.43 – 2.96 wt% were observed for the chalks and marls above the basal units

(Table 4.4).
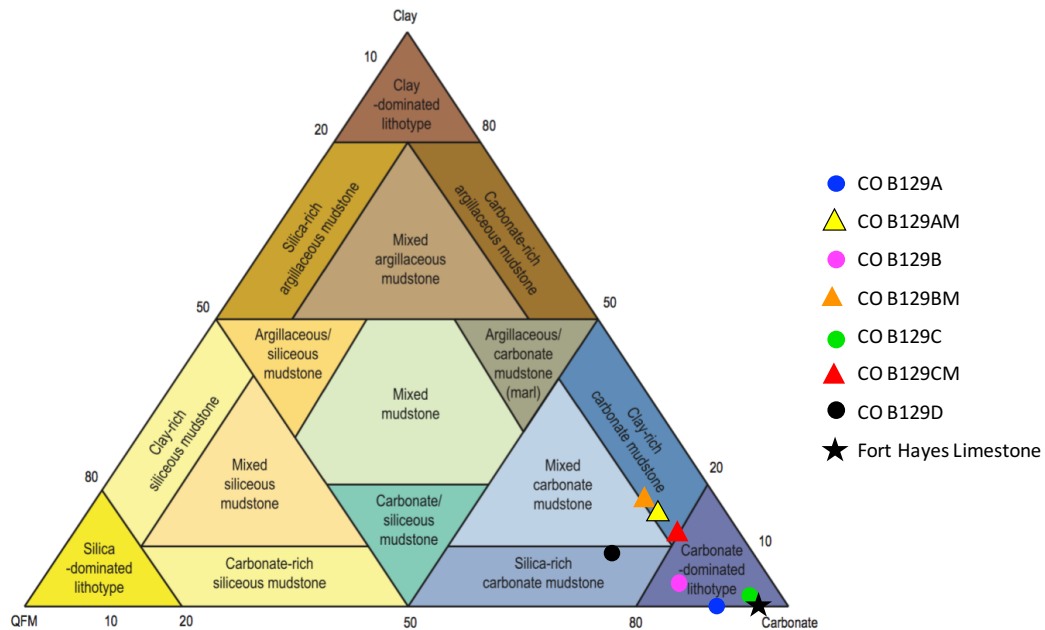
Figure 18 - sCore ternary diagram showing composition of samples from the Niobrara Formation in Berthoud State #3 well (modified from Schlumberger, 2014).

Low Pressure Gas Sorption

Niobrara samples tested typically exhibited one of two isotherm profiles

(Fig. 19-20). The characteristic shape of the adsorption curve of the isotherm

profile for chalks and marls of the Niobrara was consistent with a Type II

isotherm, which is characteristic of non-porous or predominantly macroporous

(> 50 nm) materials (Sing, 1985). Despite this classification, the Niobrara does

not produce a pure Type II isotherm, the desorption curve exhibits a type H3

hysteresis loop which suggests the samples contain a large volume of mesopores

at 2-50 nm (Sing, 1985). Since the isotherm profiles lack a plateau at higher

pressures, typically associated with type IV isotherms, they are not entirely

composed of mesopores. Materials such as the Niobrara which exhibit both

mesopores, as characterized by the type H3 hysteresis loop, and macropores, as

evident by the lack of a plateau at high pressures, are deemed Type IIB (Kuila et

al., 2012). The presence of both meso- and macropores in these samples is

consistent with the MICP results.
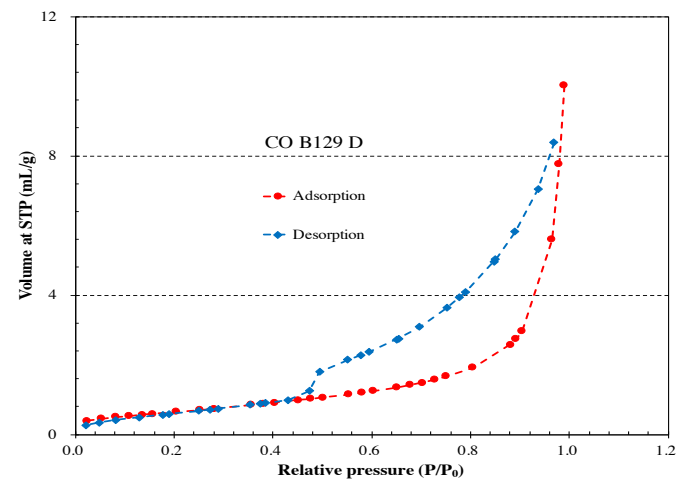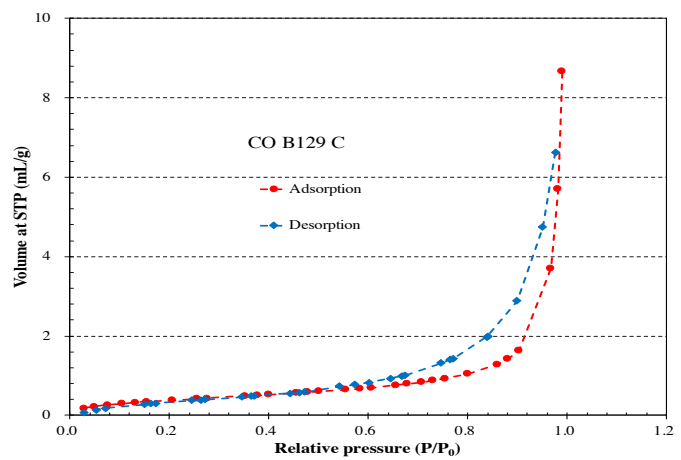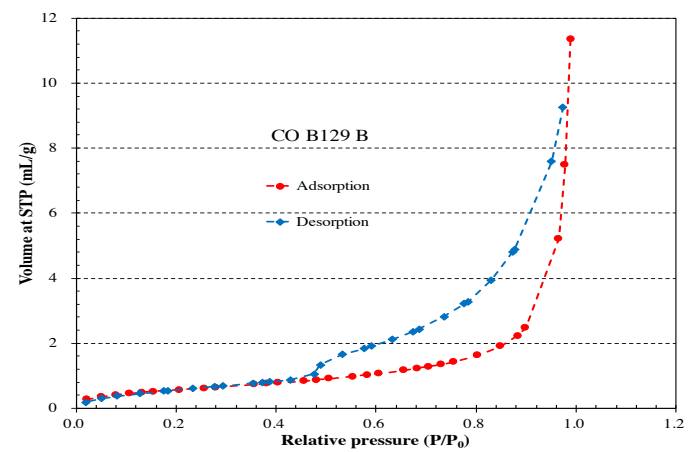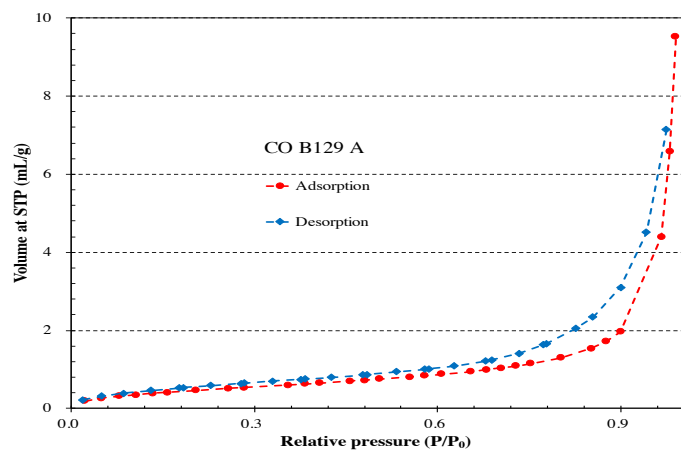
Figure 19 – Gas sorption isotherm profile of Niobrara chalks.
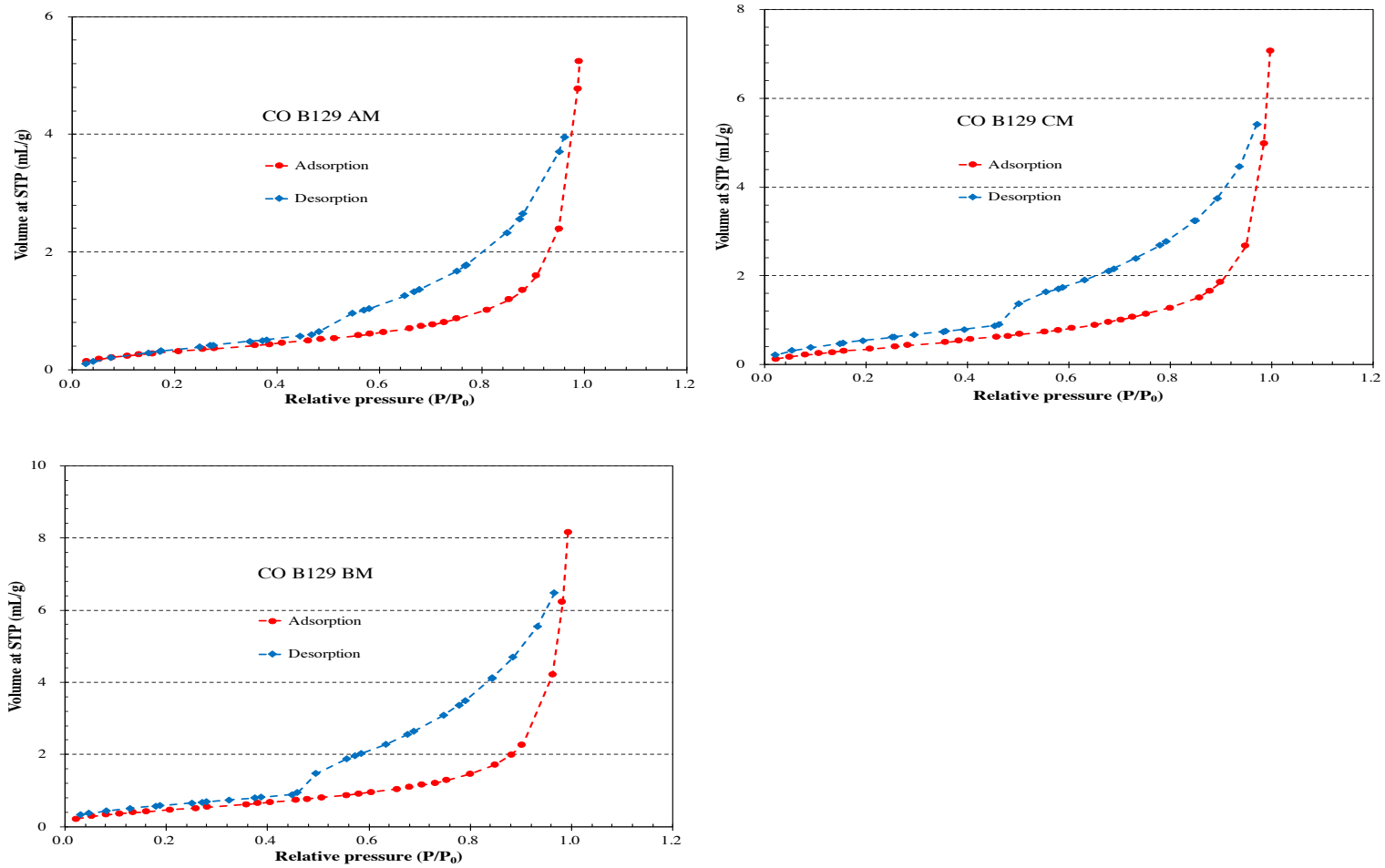
Figure 20 -– Gas sorption isotherm profile of Niobrara marls.

Multipoint BET and BJH adsorption/desorption data was obtained through low pressure gas sorption analysis (Table 4-5). With the exception of CO B129C, chalk benches, which contain less than 10% illite, within the Niobrara exhibit a higher surface area than marls (Table 4-6). Chalk samples with clay contents ranging from 0.5-7.8% show surface areas ranging from 1.83-2.42 m^2/g (excluding CO B129C). Marl samples with clay contents ranging from 10.4-15.2% had surface areas of 1.24-1.51 m^2/g. The Fort Hayes Limestone with 0% illite had the highest surface area of 2.51 m^2/g while the CO B129AM sample with 13.4% illite had the lowest surface area of 1.24 m^2/g.

Pore size distribution from the Niobrara samples were also obtained through low pressure gas sorption, ranging from 1.65 - 35.8 nm (Table 4-7). Chalks had a lower incidence of pores in the 1.65 - 5.05nm range representing 0 - 11.5% compared to 10.2 – 18.8% for marl samples. Samples CO B129A, CO B129B, CO B129C showed a bimodal pore size distribution with the majority of pores at between 5 -15 nm, whereas three marl samples exhibited a unimodal distribution with the majority of pores between 5 – 10 nm. Using the BJH method, pore sizes of 1.65 – 25 nm represented nearly 90 – 93% of all pore distribution for marl samples, yet produced smaller values of 74 - 90% for chalk samples. CO B129D, with the highest illite content of any chalk sample, had the

highest percentage of pores in the 1.65 – 5 nm (11.5%), and 90.5% of pores within 1.65 – 25 nm.

Sample ID	Multipoint BET Summary			BJH Adsorption Summary			BJH Desorption Summary		
	BET Constant	Surface Area (m^2/g)	BET Fitting R^2	Pore Volume (cc/g)	Pore Diameter Dv(d) (nm)	Surface Area (m^2/g)	Pore Volume (cc/g)	Pore Diameter Dv(d) (nm)	Surface Area (m^2/g)
CO B129A	25.1	1.83	1.000	0.015	3.18	1.65	0.015	10.9	2.24
CO B129AM	24.3	1.24	1.000	0.008	3.20	1.27	0.009	4.19	2.83
CO B129B	37.2	2.17	1.000	0.017	3.98	2.07	0.019	3.88	5.72
CO B129BM	30.9	1.79	1.000	0.013	3.01	1.91	0.014	3.84	5.85
CO B129C	30.9	1.48	1.000	0.013	2.98	1.33	0.014	4.14	2.36
CO B129CM	14.9	1.51	0.999	0.011	3.18	1.69	0.012	3.87	4.37
CO B129D	53.8	2.43	1.000	0.015	3.17	2.36	0.018	3.90	6.95
CO B129FHLS	68.3	2.51	1.000	0.01	3.01	1.80	0.01	3.87	2.74
CO B129CSS	60.6	7.91	1.000	0.023	3.14	5.55	0.025	3.88	9.91

Table 4-5– Summary of gas sorption results for samples from Niobrara Formation and Colorado Sandstone within Berthoud State #3.

Sample ID	Illite (wt%)	Surface Area (m^2/g)
CO B129A	0.5	1.832
CO B129AM	13.4	1.241
CO B129B	5.4	2.173
CO B129BM	15.2	1.792
CO B129C	1.5	1.48
CO B129CM	10.4	1.513
CO B129D	7.8	2.425
CO B129FHLS	0	2.511
CO B129CSS	5.1	7.909

Table 4-6 – Comparison of illite content with BET surface area.

Sample ID	Pore size (nm)						
	1.65-5.05	5.05-10.05	10.05-15.05	15.05-20.05	20.05-25.05	25.05-30.05	30.05-35.85
CO B129A	3.35	20.8	20.9	17.1	12.4	14.4	11.1
CO B129AM	10.2	39.1	24.4	12.3	6.78	5.37	1.78
CO B129B	5.68	32.8	26.6	14.0	7.69	6.52	6.73
CO B129BM	15.1	41.5	19.4	8.85	7.28	4.84	3.04
CO B129C	0.00	23.9	23.8	20.6	11.4	9.51	10.81
CO B129CM	18.8	34.5	18.8	9.85	7.88	5.95	4.18
CO B129D	11.5	40.1	21.2	10.2	7.56	5.84	3.69
CO B129FHLS	10.4	22.4	19.2	13.3	11.0	13.4	5.09
CO B129CSS	31.1	22.6	18.6	10.2	5.69	6.45	5.49

Table 4-7 – Pore size distribution obtained from BJH analyses of low pressure gas sorption

Imbibition

For spontaneous fluid imbibition tests on the Berthoud State #3 well, *N-*decane and DI water was used in an attempt to gauge the characteristic pore connectivity of the Niobrara samples. Fluid uptake over time was recorded on a log-log scale and slopes were obtained from each sample (Table 4-8). Typically, imbibition behavior from the Niobrara samples exhibited two slopes, but occasionally 3 slopes were observed. The first slope represents the settling of samples from initial surface contact with the imbibition fluid. The second steeper slope, which is sometimes not seen, had values ranging between 0.5-1.0 and is representative of fluid migration across well connected pores on the sample bottom and continuing up the exterior sides. The third slope is seen after roughly 60 minutes and exhibits a range of values from 0.144 – 0.319 for DI

water and 0.131 – 0.452 for *n*-decane, continuing at this value until equilibrium

is reached. Imbibition slopes around 0.25, like those seen from the Niobrara

samples, indicate a poorly connected pore network.

Sample	Testing Medium	Slope				Average Slope
		6 hours	8 hours	12 hours	24 hours	
CO B129 A	DI	0.247	—	0.208	0.151	0.202
	N-decane	—	0.397	—	—	0.397
CO B129 AM	DI	0.301	—	0.202	0.319	0.274
	N-decane	—	0.755	—	—	0.755
CO B129 B	DI	0.207	—	0.150	0.230	0.196
	N-decane	—	NA	—	—	NA
CO B129 BM	DI	0.159		0.144	0.154	0.152
	N-decane	—	0.439	—	—	0.439

Table 4-8 –IImbibition results for Niobrara samples from Berthoud State #3; for DI water, three tests with different imbibition times were conducted on the same cubic sample.

Two chalk samples which were tested, CO B129A and CO B129B, had DI

water slopes with an average value of 0.202 and 0.196, and CO B129A had an *n*-

decane slope of 0.307 (Fig. 21- 22). Sample CO B129B was not able to be tested

successfully with *n*-decane. Marl samples CO B129AM and CO B129BM

examined exhibited average slopes of 0.274 and 0.152 for DI water and *n*-

decane, and slopes of 0.755 and 0.439 respectively (Fig. 23-24).
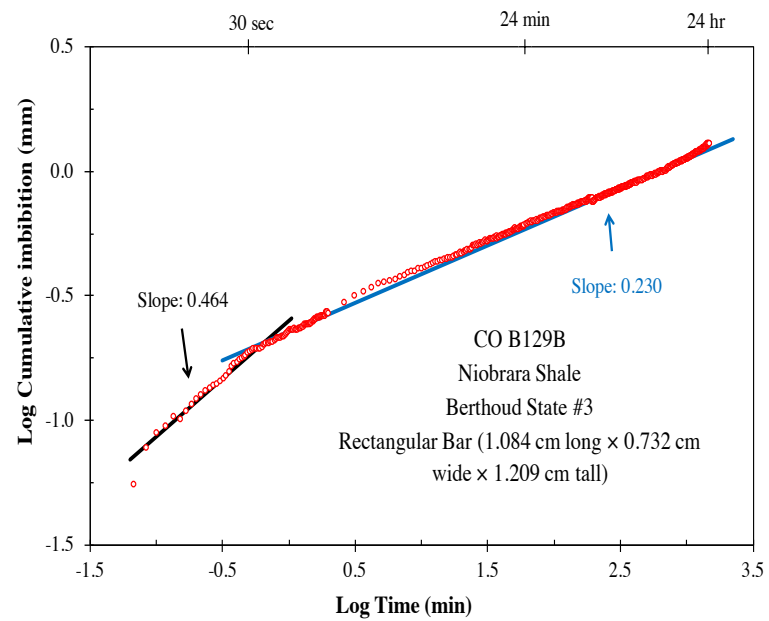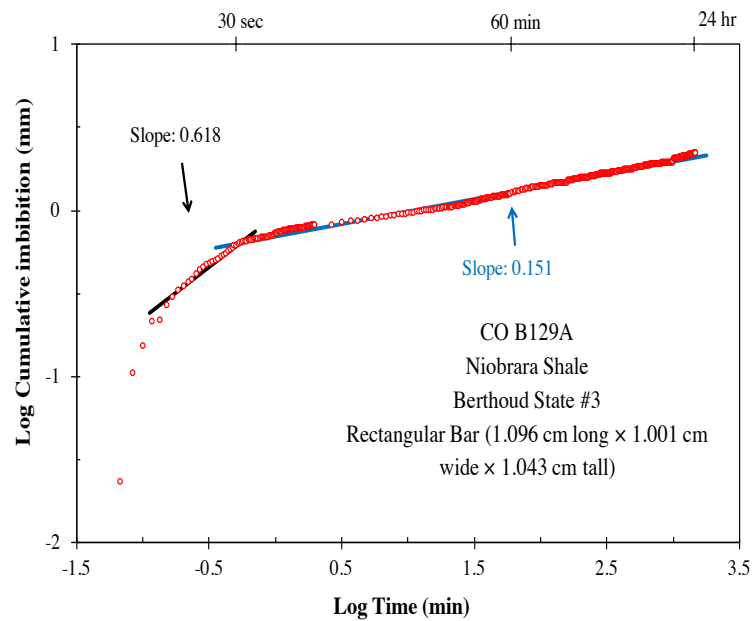
Figure 21 - 24 hr DI water imbibition tests on Niobrara chalk samples
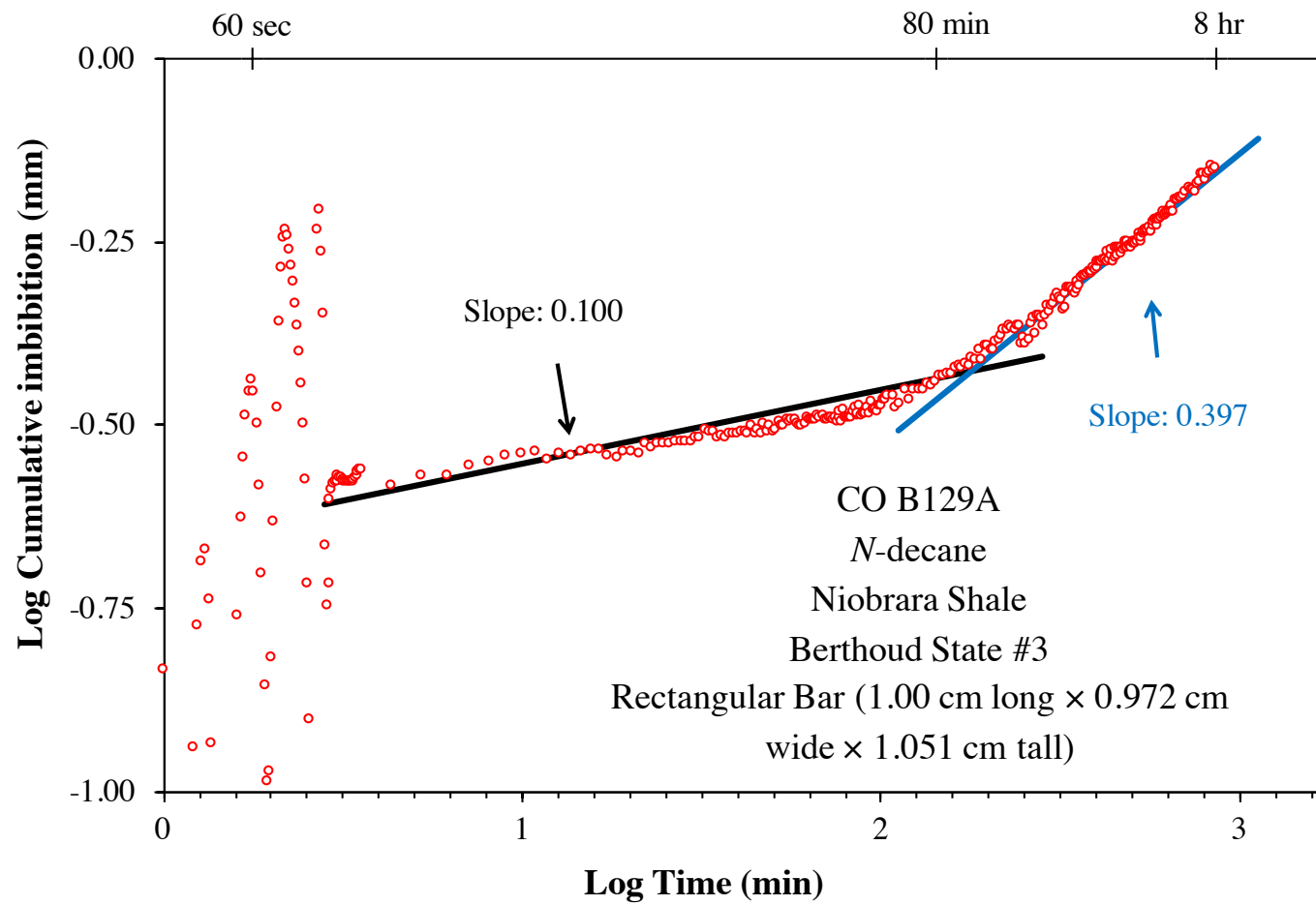
Figure 22 - 8hr *N* – decane imbibition test on Niobrara chalk
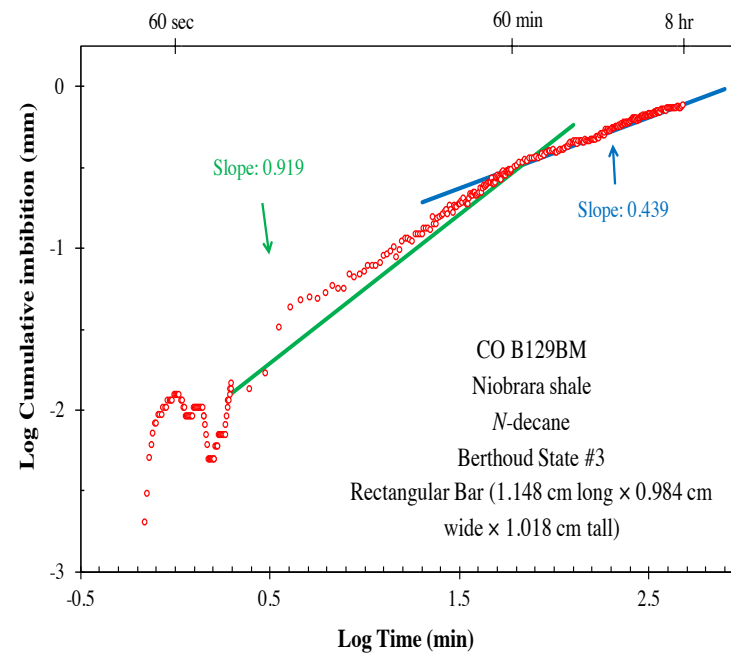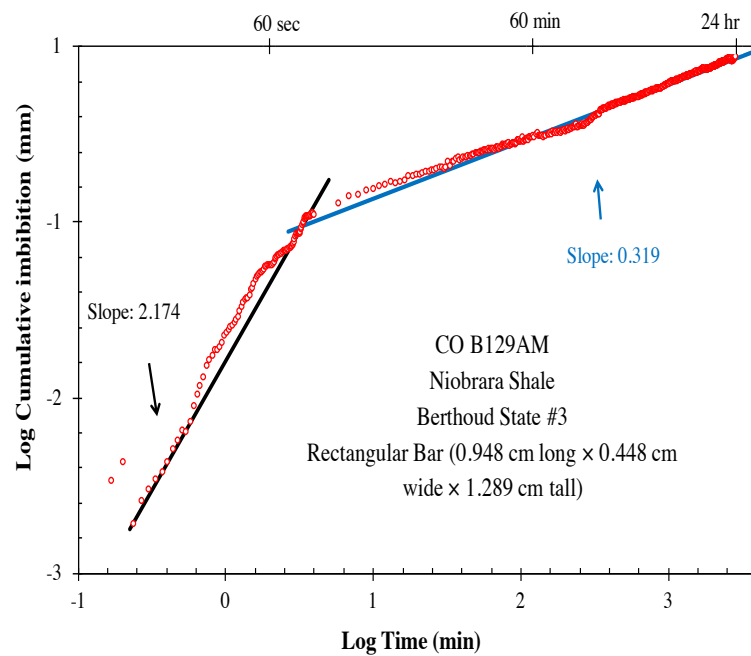
Figure 23 – 24hr DI water imbibition tests on Niobrara marl samples
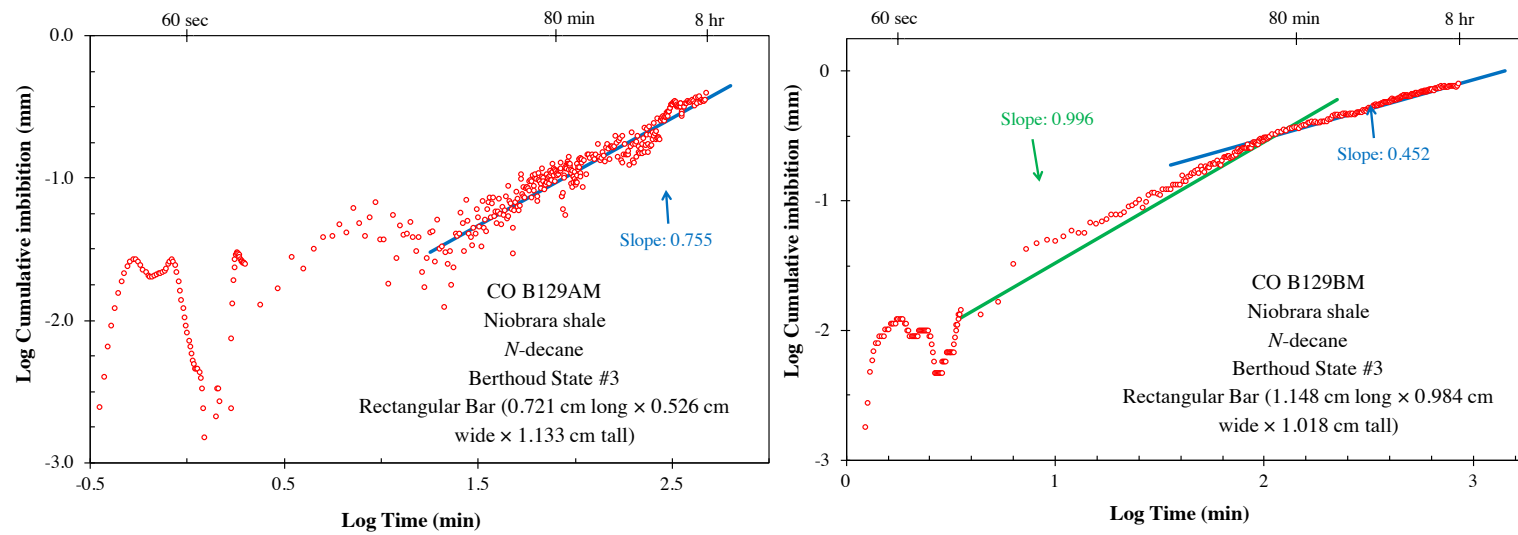
Figure 24 - 8hr *N*-decane imbibition tests on Niobrara marl samples

Vapor Adsorption

Vapor absorption tests were also conducted on Niobrara samples from Berthoud State #3 well by hanging samples above either DI water or *N*-decane. With the exception of the *N*-decane test for sample CO B129AM and CO B129BM, which were tested for a duration of 4 and 2 days respectively, tests were conducted for a duration of either 3 or 7 days dependent upon whether *n*-decane (shorter duration) or DI water was used respectively (Table 4-9). Fluid uptake over time was monitored in a similar fashion as when conducting imbibition tests, except that there is no contact between sample and fluid. Slopes for chalk samples tested with DI water ranged from 0.555 to 0.583 while *n*-decane slopes ranged from 0.338 to 0.629 (Fig. 25-26). Marl samples CO B129 AM and CO B129 BM within the Niobrara tested with DI water had slopes of 0.745 and 0.413, while *n*-decane produced slopes of 0.317 and 0.612 respectively (Fig. 27-28).

Sample	Lithology	Fluid	Duration (days)	Slope
CO B129 A	Chalk	DI	7	0.555
		N-decane	3	0.338
CO B129 AM	Marl	DI	7	0.745
		N-decane	3	0.317
CO B129 B	Chalk	DI	7	0.583
		N-decane	3	0.629
CO B129 BM	Marl	DI	7	0.413
		N-decane	3	0.614

Table 4-9 – Results from vapor adsorption tests of selected Niobrara samples from Berthoud State #3
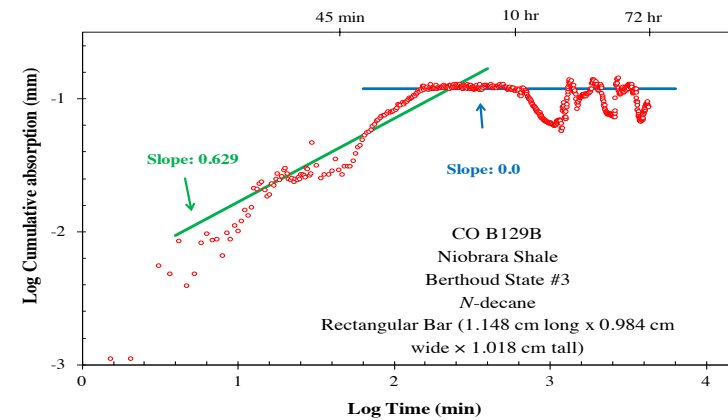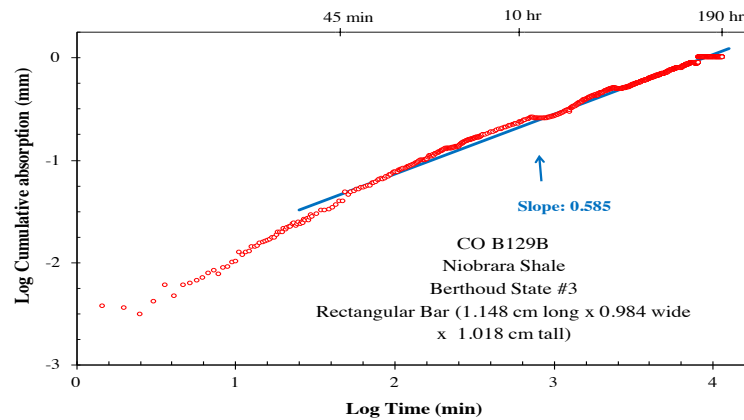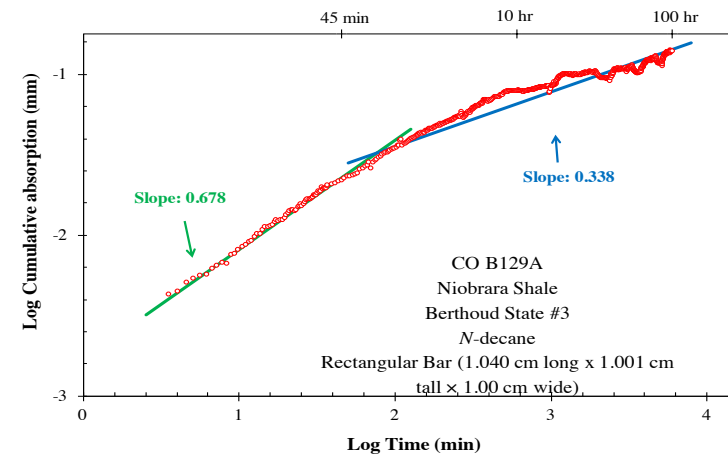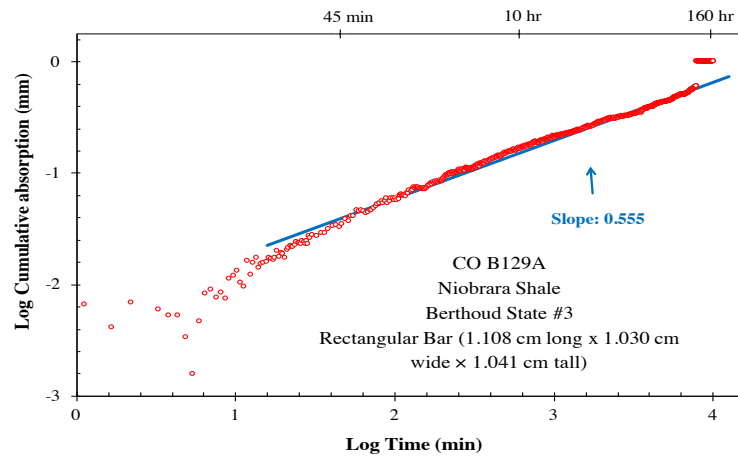
Figure 25 –Niobrara chalk samples tested through vapor adsorption using DI water for a duration of 7 days.

Figure 26 – Niobrara chalk samples tested through vapor adsorption using *N*-decane
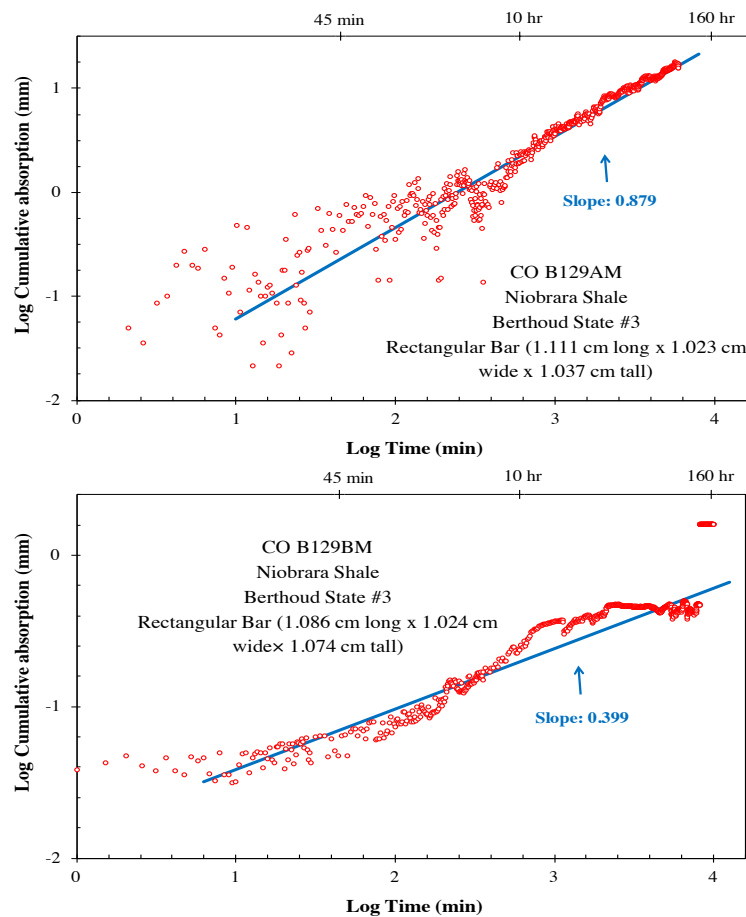
Figure 27 – Niobrara marl samples tested through vapor adsorption using DI water
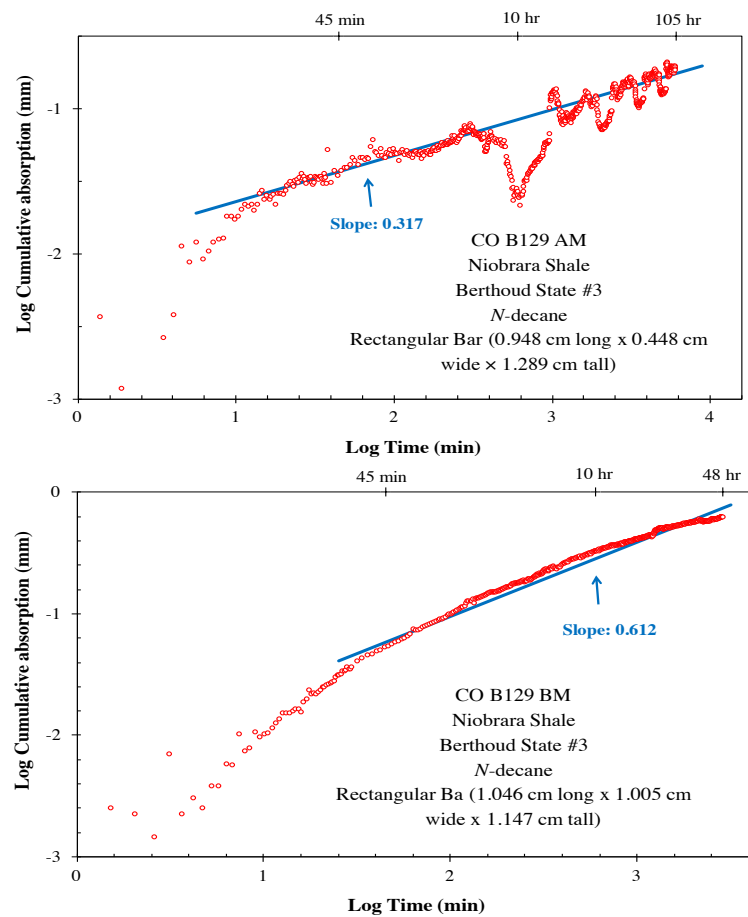
Figure 28 – Niobrara marl samples tested through vapor adsorption using *N*-decane

Chapter 5 Discussion and Conclusion

Discussion

A strong correlation was found between pore size distribution and mineralogy of the samples (Fig 20; Table 5-1). Specifically, it was noted that marl samples, which had a higher clay content (>10%), typically exhibited an increase in smaller pore sizes in the 3-5 nm range. CO B129D, had the highest clay content of any of the chalk samples at 7.8%, and showed the highest presence of pores in the 3-5nm range of any chalk samples. Conversely, samples with higher calcite content had a higher incidence of larger pores in the 5-50 nm range. Samples CO B129A, CO B129C, and CO B129FHLS which had the lowest weight percentage of illite and highest percentages of calcite (~90-94%) had the majority of their pores within the 10-50nm range. Although the sample size used for these tests was somewhat small, the findings are consistent with those of Kulia (2012), suggesting illite content may be a deciding factor in pore size distribution.

Most benches within the Niobrara Formation of Berthoud State #3 well exhibited unimodal pore size distribution from MICP analyses, however, CO B129 BM, which exhibited the highest illite content of all tested samples, had bi-modal pore size distribution with 31% and 45% of all pores occurring in 3-5nm and 5-10nm respectively. The propensity of illite samples to have an increased

49

incidence of pores in the 3-5nm range, when compared to samples with lower clay content, suggests illite may reduce intra and inter pore spaces within the samples.
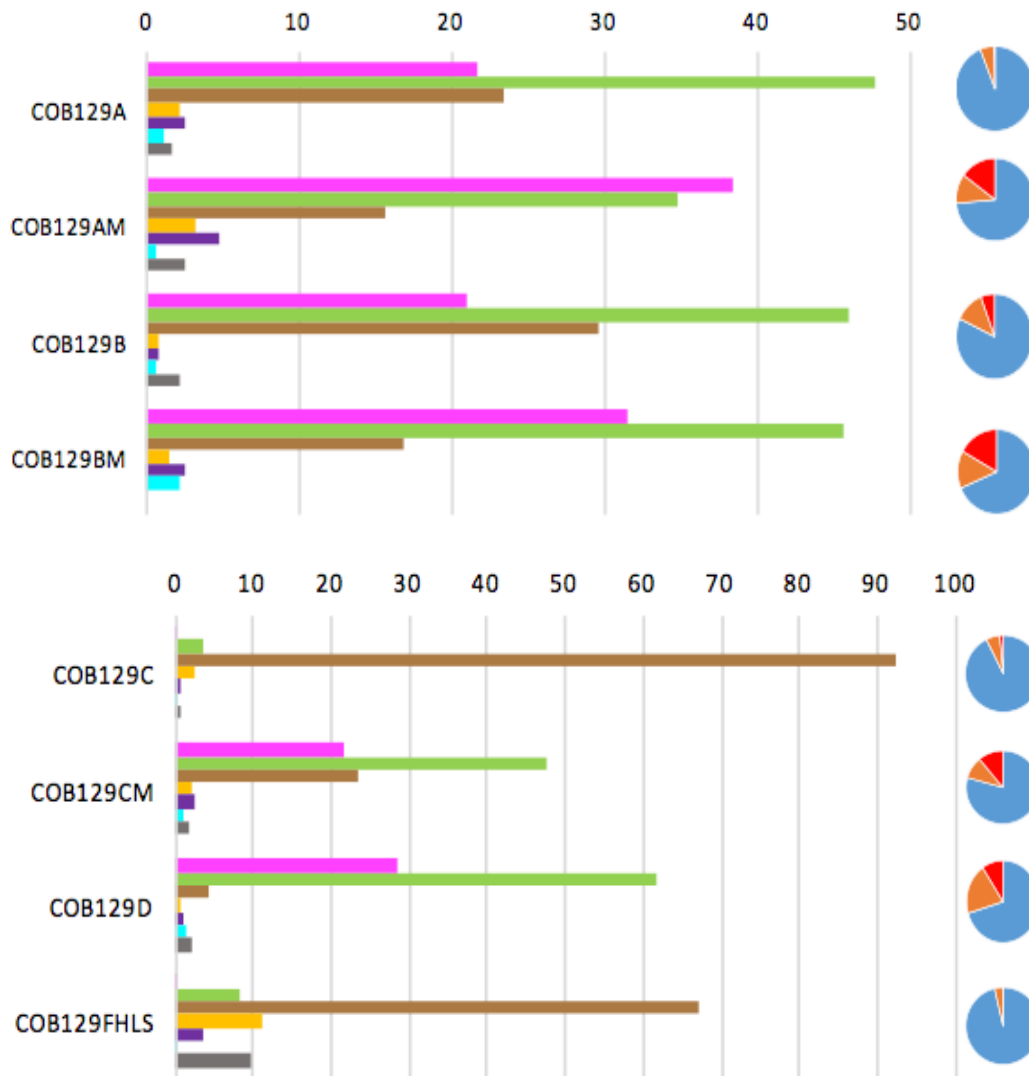
Figure 29 – Mineralogy compared to pore size distribution

Sample ID	3-5nm Pores (%)	Illite (wt%)
CO B129A	21.574	0.5
CO B129AM	38.453	13.4
CO B129B	20.982	5.4
CO B129BM	31.468	15.2
CO B129C	0.17	1.5
CO B129CM	21.574	10.4
CO B129D	28.533	7.8
CO B129FHLS	0.034	0
CO B129CSS	4.361	5.1

Table 5-1 – Prevalence of 3-5 nm pores in comparison to illite (wt%)

Illite content also appears to play a key role in porosity of the samples with an R^2 value of 0.88 (Fig. 30). The horizontal axis of Fig. 31 shows chalk samples to the left and marl samples to the right, and a clear correlation can be seen between illite content and sample porosity. Samples with the lowest clay content (<10%), such as CO B129A with 0.5% illite, had the highest porosity of all samples tested at 8.4%. CO B129AM, only 63 feet from CO B129A, had one of the highest illite (13.4%) contents of all samples tested, and consequently had the lowest porosity seen of only 2.1%. Similar to illite reducing intra and inter pore spaces causing a higher incidence of pores in the 3-5nm range, in this instance illite has effectively reduced porosity within the pore network.
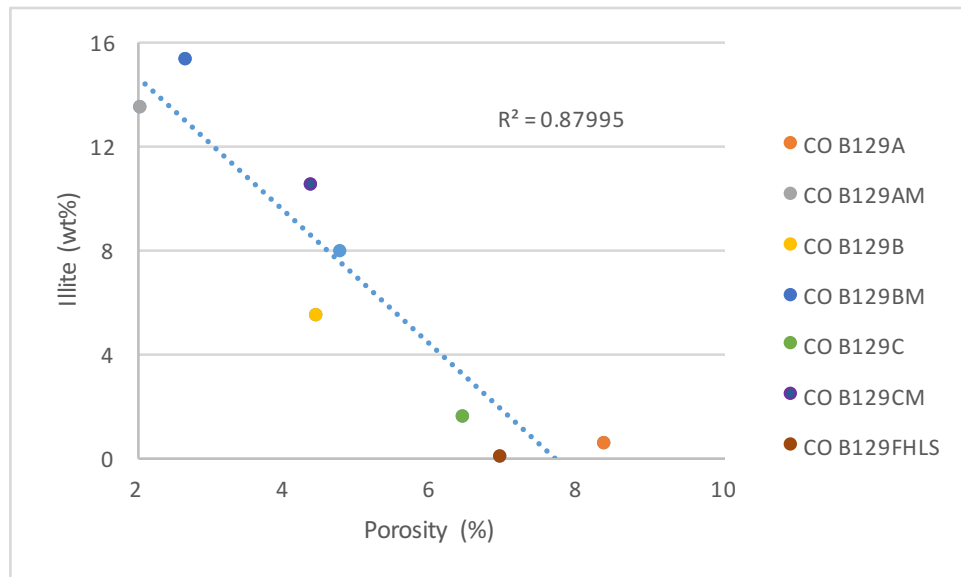
Figure 30 - Porosity compared to illite content with an R^2 value of 0.87
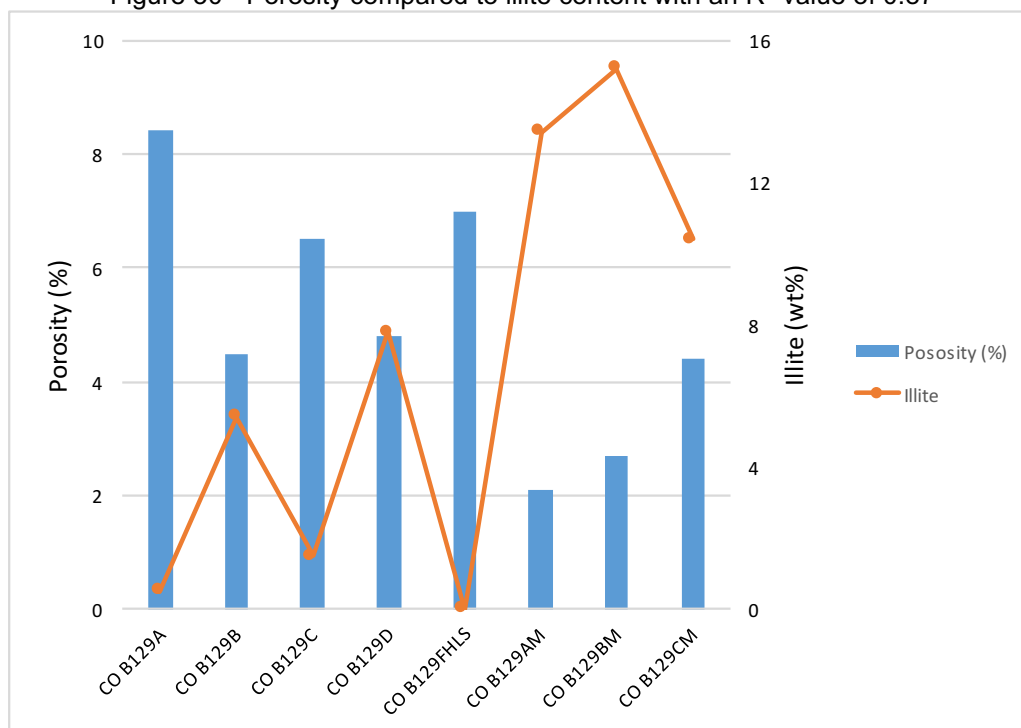
Figure 31– Porosity compared to illite percentage. Niobrara chalks are on the left side of the graph and chalks are on the right.

Conclusion

The objective of this study was to gain a better understanding of the pore

network within the Niobrara formation of Berthoud State #3 well. Wettability

tests were first conducted to determine whether samples were water wet or oil

wet utilizing DI water, 10% IPA, *n*-decane, and API Brine. Through these tests it

was determined samples were hydrophobic, to readily adsorb the oil-wetting n-

decane. Imbibition tests produced slopes of roughly 0.25 for both fluids of DI

water and n-decane, suggesting a rather poorly connected pore network, even

though the samples are wetting to n-decane. MICP tests were conducted on all

samples to better understand the pore-throat size distribution and allowed an

understanding of pores ranging in size from 2.8 nm to 50 μm you had 36 earlier.

Through MICP it was found that chalks had a tendency for larger pores in the 5-

50 nm range, whereas marl samples exhibited a much greater incidence of pores

in the 2.8-5 nm range when compared to chalk samples.

When comparing mineralogical composition from XRD results with gas

sorption and MICP results, a distinct correlation was found between clay

composition, pore size distribution, and porosity. Samples with the highest illite

content exhibited lowest porosities and had the highest incidence of pores in the

2.8-5 nm range. In addition, porosities of these same samples were the lowest

of any seen ranging from 2.2-4.4%.

In the Niobrara, illite content seems to be the determining factor in pore

size distribution. Samples with greater than 10% illite consistently produced a

greater amount of pores in the 2.8-5nm range in comparison to those with lower

illite content. Porosity of those same samples with higher illite content was also

decreased in comparison to samples with lower clay content. These results

suggest samples which have higher illite concentrations (>10%) have a higher

propensity to reduce intra and inter pore spaces causing a decrease in porosity

and a higher incidence of pores in the 2.8-5nm range.

Recommendations

In order to validate the results found in this study, additional research

needs to be conducted within the Niobrara throughout its expanse.

Furthermore, similar studies need to be conducted in other plays such as the

Eagle Ford, Wolfcamp, Bakken and Marcellus. A better understanding of pore

size distribution in unconventional reservoirs throughout the country could

eventually lead to increased production and reduce overall associated costs.

References

Anderson, D., M. Nobakht, S. Moghadam, and L. Mattar. 2010. Analysis of

Production Data From Fractured Shale Gas Wells: *Proceedings of SPE*

Unconventional Gas Conference, doi:10.2523/131787-ms.

Asquith, G. B., C. R. Gibson, S. Henderson, N. F. Hurley, and D. Krygowski. 2004.

Basic well log analysis: Tulsa, OK, *American Association of Petroleum*

Geologists.

Barlow, L.K., and E.G. Kauffman. 1985. Depositional cycles in the Niobrara
Formation, Colorado Front Range: SEPM Field Trip Guidebook, 4: 199-208.
doi:10.2110/sepmfg.04.199.

Barrett, E. P., L. G. Joyner, and P. P. Halenda. 1951. The Determination of Pore

Volume and Area Distributions in Porous Substances. I. Computations from

Nitrogen Isotherms: *Journal of the American Chemical Society*, 73(1): 373–

380, doi:10.1021/ja01145a126.

Bobko, C., and F.-J. Ulm. 2008. The nano-mechanical morphology of shale:

Mechanics of Materials, 40(4-5): 318–337,

doi:10.1016/j.mechmat.2007.09.006.

Borysenko, A., B. Clennell, R. Sedev, I. Burgar, J. Ralston, M. Raven, D. Dewhurst,

and K. Liu. 2009. Experimental investigations of the wettability of clays and

shales: *Journal of Geophysical Re*search, 114(B7), doi:10.1029/2008jb005928.

Blakey, R., 2011. *Western Interior Cretaceous Basin, Late Cretaceous, 85 Ma:*

North American Paleogeographic Maps. Available at

http://jan.ucc.nau.edu/~rcb7/namK85.jpg. Accessed 4 April 2016.

Brown, C., J. Crafton, and J. Golson. 1982. The Niobrara Gas Play: Exploration and

Development of a Low-Pressure, Low-Permeability Gas Reservoir: *Journal of*

Petroleum Technology, 34(12): 2863–2870, doi:10.2118/10304-pa.

Brunauer, S., P. H. Emmett, and E. Teller. 1938. Adsorption of Gases in

Multimolecular Layers: *Journal of the American Chemical Society*, 60(2): 309–

319, doi:10.1021/ja01269a023.

Bustin, A. M., and R. M. Bustin. 2012. Importance of rock properties on the

producibility of gas shales: *International Journal of Coal Geology*, 103: 132–

147, doi:10.1016/j.coal.2012.04.012.

Chalmers, G. R., D. J. Ross, and R. M. Bustin. 2012. Geological controls on matrix

permeability of Devonian Gas Shales in the Horn River and Liard basins,

northeastern British Columbia, Canada: *International Journal of Coal*

Geology, 103: 120–131, doi:10.1016/j.coal.2012.05.006.

Chong, K. K., W. Grieser, O. Jaripatke, and A. Passman. 2010. A Completions

Roadmap to Shale-Play Development: A Review of Successful Approaches

toward Shale-Play Stimulation in the Last Two Decades: Proceedings of

International Oil and Gas Conference and Exhibition in China, doi:10.2523/130369-ms.

Chukwuma, F. 2015. Nanopetrophysics of the Utica Shale, Appalachian Basin, Ohio, USA. M.S. Thesis, Department of Science, University of Texas at Arlington, USA.

Dong, J.-J., J.-Y. Hsu, W.-J. Wu, T. Shimamoto, J.-H. Hung, E.-C. Yeh, Y.-H. Wu, and H. Sone. 2010. Stress-dependence of the permeability and porosity of sandstone and shale from TCDP Hole-A: *International Journal of Rock Mechanics and Mining Sciences*, 47(7): 1141–1157, doi:10.1016/j.ijrmms.2010.06.019.

EIA (Energy Information Administration). 2015. *U.S. oil production growth in 2014 was largest in more than 100 years*. Released on March 30, 2015. Available at http://www.eia.gov/todayinenergy/detail.cfm?id=20572#. Accessed 7 April 2016.

Ewing, R. P., and R. Horton. 2002. Diffusion in sparsely connected pore spaces: Temporal and spatial scaling: *Water Resources Research*, 38(12), doi:10.1029/2002wr001412.

Fessler D. 2011. *Forget Shale Gas: Shale Oil is the New Energy Boom in the United States.* Released on November 8, 2011. Available at

http://www.investmentu.com/article/detail/25041/shale-oil-the-new-energy-boom#.V88Z4WVY9FI. Accessed August 29, 2016.

Hanley, E. J., and L. E. Vanhorn. 1982. Niobrara Development Program, Washington County, CO: *Journal of Petroleum Technology*, 34(3): 628–634, doi:10.2118/9850-pa.

Hashmet, M. R., I. M. Tan, S. Majidaei, and M. Mushtaq. 2012. Simultaneous Determination of Capillary Pressure and Relative Permeabilities: *SPE Saudi Arabia Section Technical Symposium and Exhibition*, doi:10.2118/160878-ms.

Hattin, D. E., 1981. Petrology of Smoky Hill Member, Niobrara Chalk (Upper Cretaceous), in Type Area, Western Kansas: *AAPG Bulletin*, 65, doi:10.1306/2f919b11-16ce-11d7-8645000102c1865d.

Hu, Q., and R. Ewing. 2014. Integrated experimental and modeling approaches to studying the fracture-matrix interaction in gas recovery from Barnett Shale. Final Report, Research Partnership to Secure Energy for America (RPSEA), National Energy Technology Laboratory, Department of Energy, 91p.

Hu, Q., R. P. Ewing, and S. Dultz. 2012. Low pore connectivity in natural rock: *Journal of Contaminant Hydrology*, 133: 76–83, doi:10.1016/j.jconhyd.2012.03.006.

Hu, Q.H., X.B. Gao, Z.Y. Gao, R.P. Ewing, S. Dultz, and J. Kaufmann. 2014. Pore

accessibility and connectivity of mineral and kerogen phases in shales. Presentation at the Unconventional Resources Technology Conference held in Denver, Colorado, USA, 25–27 August 2014. URTeC 1922943.

Hu, Q.-H., X.-G. Liu, Z.-Y. Gao, S.-G. Liu, W. Zhou, and W.-X. Hu. 2015a. Pore structure and tracer migration behavior of typical American and Chinese shales: *Petroleum Science*, 12(4): 651–663, doi:10.1007/s12182-015-0051-8.

Hu, Q., R. P. Ewing, and H. D. Rowe. 2015b. Low nanopore connectivity limits gas production in Barnett formation: Journal of Geophysical Research: *Solid Earth*, 120(12): 8073–8087, doi:10.1002/2015jb012103.

Hughes, J.D., 2014. Drilling Deeper: A Reality Check on U.S. Government Forecasts for a Lasting Oil and Shale Gas Boom. *Post Carbon Institute*.

Josh, M., L. Esteban, C. D. Piane, J. Sarout, D. Dewhurst, and M. Clennell. 2012. Laboratory characterization of shale properties: *Journal of Petroleum Science and Engineering*, 88-89: 107–124, doi:10.1016/j.petrol.2012.01.023.

Kauffman, E.G., 1969. Cretaceous marine cycles of the Western Interior. *Mountain Geologist*, 6(4): 227-245.

Kauffman, E.G., 1977. Geological and biological overview: Western Interior Cretaceous basin. *Mountain Geologist*, *14*(3-4): 75-99.

Kauffman, E.G. and Caldwell, W.G.E., 1993. The Western Interior Basin in space and time. *Evolution of the Western Interior Basin: Geological Association of Canada, Special Paper*, *39*: 1-30.

Kaufmann, J., 2010. Pore space analysis of cement-based materials by combined Nitrogen sorption – Wood's metal impregnation and multi-cycle mercury intrusion: *Cement and Concrete Composites*, 32(7): 514–522, doi:10.1016/j.cemconcomp.2010.04.003.

Konishi, T., and H. Sues. 2012. The northernmost occurrence of Prognathodon (Squamata: Mosasauridae) from the Western Interior Seaway of North America: *Canadian Journal of Earth Sciences*, 49(9): 1111–1115, doi:10.1139/e2012-038.

Kuila, U., M. Prasad, A. Derkowski, and D. K. Mccarty. 2012. Compositional Controls on Mudrock Pore-Size Distribution: An Example from Niobrara Formation: SPE Annual Technical Conference and Exhibition, doi:10.2118/160141-ms.

Kuila, U., and M. Prasad. 2013. Specific surface area and pore-size distribution in clays and shales: *Geophysical Prospecting*, 61(2): 341–362, doi:10.1111/1365-2478.12028.

Li, K., 2007. Scaling of spontaneous imbibition data with wettability included:

    Journal of Contaminant Hydrology, 89(3-4): 218–230,

    doi:10.1016/j.jconhyd.2006.09.009.

Locklair, R. E., and B. B. Sageman. 2008. Cyclostratigraphy of the Upper

    Cretaceous Niobrara Formation, Western Interior, U.S.A.: A Coniacian–

    Santonian orbital timescale: *Earth and Planetary Science Letters*, 269(3-4):

    540–553, doi:10.1016/j.epsl.2008.03.021.

Longman, M.W., B.A. Luneau, and S.M. Landon. 1998. Nature and distribution of

    Niobrara lithologies in the Cretaceous Western Interior Seaway of the Rocky

    Mountain region. *Mountain Geologist*, *35*: 137-170.

Lopez, R., A. Soria. 2007. Kinematical description of the spontaneous imbibition

    processes. IASME/WSEAS international conference, Athens, Greece.

Luneau, B., M. Longman, P. Kaufman, and S. Landon. 2011. Stratigraphy and

    petrophysical characteristics of the Niobrara formation in the Denver basin,

    Colorado and Wyoming. *Search and Discovery Article*, *50469*.

Metwally, Y. M., and C. H. Sondergeld. 2011. Measuring low permeabilities of

    gas-sands and shales using a pressure transmission technique: *International*

    Journal of Rock Mechanics and Mining Sciences, 48(7)7: 1135–1144,

    doi:10.1016/j.ijrmms.2011.08.004.

Micrometrics. 2011. Autopore IV 9500 Operators Manual.

Morrow, N. R., and X. Xie. 2001. Oil recovery by spontaneous imbibition from

    weakly water-wet rocks. *Petrophysics*, *42*(04): 313-322.

Nielsen, K. S., C. J. Schröder-Adams, D. A. Leckie, J. W. Haggart, and K. Elberdak.

    2008. Turonian to Santonian paleoenvironmental changes in the Cretaceous

    Western Interior Sea: The Carlile and Niobrara formations in southern

    Alberta and southwestern Saskatchewan, Canada: *Palaeogeography,*

    Palaeoclimatology, Palaeoecology, 270(1-2): 64–91,

    doi:10.1016/j.palaeo.2008.08.018.

Potter, P. E., J. B. Maynard, and W. A. Pryor. 1980. Sedimentology of shale: study

    guide and reference source: New York, Springer-Verlag.

Prasad, M., K. C. Mba, T. Sadler, and M. L. Batzle. 2009. Maturity and Impedance

    Analyses of Organic-Rich Shales: SPE Rocky Mountain Petroleum Technology

    Conference, doi:10.2118/123531-ms.

Pratt, L.M., E.G. Kauffman, and F.B. Zelt. 1985. *Fine-grained deposits and*

    biofacies of the Cretaceous Western Interior Seaway: evidence of cyclic

    sedimentary processes (No. 4). Sepm Society for Sedimentary.

Ravikovitch, P. I., G. L. Haller, and A. V. Neimark. 1998. Density functional theory

    model for calculating pore size distributions: pore structure of nanoporous

    catalysts: *Advances in Colloid and Interface Science*, 76-77: 203–226,

    doi:10.1016/s0001-8686(98)00047-5.

Rezaee, R., A. Saeedi, and B. Clennell. 2012. Tight gas sands permeability
estimation from mercury injection capillary pressure and nuclear magnetic
resonance data: *Journal of Petroleum Science and Engineering*, 88-89: 92–99,
doi:10.1016/j.petrol.2011.12.014.

Runnels, R.T. and I.M Dubins. 1949. Chemical and petrographic studies of the
Fort Hays Chalk in Kansas.

Sahini, M. and M. Sahimi.1994. Applications of percolation theory. CRC Press.

Scholle, P.A., D.G. Bebout, and C.H. Moore. 1983. Carbonate Depositional
Environments: *AAPG Memoir 33*.

Scott, G. R., and W. A. Cobban. 1964. Stratigraphy of the Niobrara Formation at
Pueblo, Colorado. *United States Geological Survey Professional Paper*, 454-L:
1-30.

Shurr, G. W., G.A. Ludvigson, and R.H. Hammond. 1994. Perspectives on the
Eastern Margin of the Cretaceous Western Interior Basin. *Geological Society
of America Special Papers,* 287: 264-287.

Sing, K. S. W., 1985. Reporting physisorption data for gas/solid systems with
special reference to the determination of surface area and porosity: *Pure and
Applied Chemistry*, 57(4): 603–619, doi:10.1351/pac198557040603.

Sonnenberg, S.A., 2012. The Niobrara Petroleum System, Rocky Mountain

Region. *AAPG Article*, *80206*.

Środoń, J., 2001. Quantitative X-Ray Diffraction Analysis of Clay-Bearing Rocks

from Random Preparations: *Clays and Clay Minerals*, 49(6): 514–528,

doi:10.1346/ccmn.2001.0490604.

Standnes, D.C. and T. Austad. 2000. Wettability alteration in chalk: 2. Mechanism

for wettability alteration from oil-wet to water-wet using surfactants. *Journal

of Petroleum Science and Engineering*, *28*(3): 123-143.

Stauffer, D., and A. Aharony. 1994. Introduction to percolation theory: London,

Taylor&Francis.

Stright, D., and R. Robertson. 1995. An Integrated Approach to Evaluation of

Horizontal Well Prospects in the Niobrara Shale: *SPE Reservoir Engineering*,

10(4): 247–252, doi:10.2118/25923-pa.

Ulm, F.-J., and Y. Abousleiman. 2006. The nanogranular nature of shale: *Acta

Geotech*nica, 1(2): 77–88, doi:10.1007/s11440-006-0009-5.

Wang, D., R. Butler, H. Liu, and S. Ahmed. 2011. Flow-Rate Behavior and

Imbibition in Shale: *SPE Reservoir Evaluation & Engineering*, 14(4): 485–492,

doi:10.2118/138521-pa.

Washburn, E. W., 1921. Note on a Method of Determining the Distribution of

Pore Sizes in a Porous Material: *Proceedings of the National Academy of*

Sciences, 7(4): 115–116, doi:10.1073/pnas.7.4.115.

Biographical Information

Rafael Roberto Villegas, was born in San Antonio, Texas, to Dr. Rafael and Norma Villegas. He received his Bachelor's Degree in Biology from Texas A&M University Kingsville in 2005. After working for several years, Rafael decided it was time for a career change and began to pursue his Master's Degree in Petroleum Geosciences at the University of Texas at Arlington, UTA. During his studies at UTA he took an interest in petrophysics and collaborated with the C3PM research group under the leadership of Dr. Q.H. Hu. Throughout his academic career, Rafael was active with the Fort Worth and Dallas Geological Societies and attended numerous conferences and seminars dealing with petrophysics of unconventional reservoirs. After graduation, Rafael intends to enter into the oil and gas industry as a petroleum geologist.